Technische Universität Ilmenau
Institut für Mathematik

Preprint No. M 04/12

Continuation of Quasiperiodic Invariant Tori

Schilder, Frank; Osinga, Hinke M.; Vogt, Werner

Oktober 2004

Impressum:
Hrsg.: Leiter des Instituts für Mathematik
Weimarer Straße 25
98693 Ilmenau
Tel.: +49 3677 69 3621
Fax: +49 3677 69 3270
http://www.tu-ilmenau.de/ifm/

ISSN xxxx-xxxx

ilmedia

Continuation of Quasiperiodic Invariant Tori

Frank Schilder* Hinke M. Osinga Werner Vogt

26th October 2004

Abstract

Many systems in science and engineering can be modelled as coupled or forced nonlinear oscillators, which may possess quasi-periodic or phase-locked invariant tori. Since there exist routes to chaos involving the break-down of invariant tori, these phenomena attract considerable attention. This paper presents a new algorithm for the computation and continuation of quasi-periodic invariant tori of ordinary differential equations that is based on a natural parametrisation of such tori. Since this parametrisation is uniquely defined, the proposed method requires neither the computation of a base of a transversal bundle, nor re-meshing during continuation. It is independent of the stability type of the torus and examples of attracting and saddle-type tori are given. The algorithm is robust in the sense that it can compute approximations to weakly resonant tori. The performance of the method is demonstrated with examples.

Key words. invariant tori, continuation, invariance condition, finite-difference method

AMS subject classifications. 37M99 (37D10, 37M20, 65L99, 65P05)

Contents

*Supported by EPSRC grant GR/R72020/01.

1 Introduction

Coupled or forced oscillators occur in many applications as far ranging as aerodynamics and chemical reactions; we refer, for example, to [32] as an entry point to the extensive literature. These oscillators can exhibit quasiperiodic oscillations, that is, oscillations with at least two (incommensurate) internal frequencies [6, 8, 9, 48, 61]. Recent fields of applications in which quasiperiodic oscillations were reported include laser dynamics [3, 45, 46], rotor dynamics of jet engines [5], power networks [14, 37] and population dynamics in chemostats [49].

A quasiperiodic oscillation (motion) takes place on a quasiperiodic invariant torus which is densely filled by quasiperiodic orbits [8, 61]. In this paper we consider the computation and continuation of quasiperiodic invariant tori of ordinary differential equations (ODEs) of the form

$$\dot{x} = f(x,\lambda)\,, \qquad f : \mathbb{R}^n \times \mathbb{R}^m \to \mathbb{R}^n\,,\ \ n \geq 3\,,\ \ m \geq 1\,. \tag{1}$$

Here $\lambda \in \mathbb{R}^m$ is a parameter and we always assume that f is sufficiently smooth. We assume that (1) has a family of sufficiently smooth p-dimensional quasiperiodic invariant tori with $m \geq p$. This means that in the parameter space exist differentiable manifolds of codimension $p-1$ for which the flow on the tori is equivalent, that is, the rotation vector $\varrho = (\omega_2/\omega_1, \ldots, \omega_p/\omega_1)$ is constant, where $\omega = (\omega_1, \ldots, \omega_p)$ are the (unknown) internal frequencies; see §3.2. The union of these manifolds constitutes a Cantor-like set of parameter values for which quasiperiodic invariant tori exist; [6, 8, 9, 48].

In this paper we propose a *natural parametrisation* of a quasiperiodic invariant torus, which leads to a specific invariance equation; see §3. An easy-to-implement algorithm is derived by discretising this invariance equation using finite-differences. This discretisation can be constructed by recursion over the dimension p of the torus; see §4.2. Therefore, our implementation can be used for the computation of quasiperiodic invariant tori of arbitrary fixed dimension p, the limiting factor being only the available computational power. Since the parametrisation is uniquely defined, the proposed algorithm is naturally suited for continuation and is incorporated into a p-parameter pseudo-arclength continuation algorithm. Even though the derivation of the algorithm applies to the quasiperiodic case, we find that it can also be used to follow a branch of invariant tori in one parameter, that is, even when the tori are resonant, provided the encountered resonances are 'weak enough'; see §4.3 for details. Peaks in the estimated error, which is monitored during continuation, can actually be used to locate Arnol′d tongues. The algorithm works independently

of the stability-type of the torus. It is able to 'step over' small parameter values or intervals, respectively, where the torus changes stability; see §5.3 for an example.

This paper is organised as follows. In §2 we give an overview of the historical background of methods for the computation of invariant tori. (This section is independent from the rest of the paper.) Section §3 covers the derivation of an invariance equation for quasiperiodic invariant tori. Its discretisation by finite differences is described in detail in §4. In §5 we demonstrate the performance of our algorithm with examples. In particular, an example is given where a torus changes stability and a family of period-doubled tori emerges; see §5.3.

2 Historical Background

The first direct numerical approximations of invariant 2-tori appeared in the engineering literature about 25 years ago. Since quasiperiodic invariant 2-tori of dynamical systems can be observed directly as the closure of a quasiperiodic orbit, early attempts of the numerical investigation of quasiperiodic invariant 2-tori were based on the computation of quasiperiodic orbits. Chua and Ushida [17] described in 1981 the *spectral balance method* for the approximation of quasiperiodic orbits, which is a generalisation of the *harmonic balance method* used for the approximation of periodic orbits. A description of both methods can be found in [56]. The basic idea is to use Fourier polynomial approximations for a quasiperiodic orbit, where the set of base functions must be chosen carefully to avoid small divisor problems. The Fourier coefficients are computed by comparison of coefficients of the base functions, which is essentially the Fourier-Galerkin method. A similar idea was used by Díez, Jorba and Simó [22, 31] in 1991. The main difference, from a numerical point of view, is that the Fourier coefficients are computed using collocation instead of comparison of coefficients. Both methods are suitable for the approximation of quasiperiodic orbits regardless of their stability type. We use a similar idea in §5.3 for obtaining initial approximations to the 2-torus and its second basic frequency.

Another approach for the numerical analysis of quasiperiodic orbits was introduced by Kaas-Petersen [41, 42, 43] in 1985; see also [64]. Here, a quasiperiodic orbit is computed as a fixed point of a generalised Poincaré map. This algorithm is generalisable to quasiperiodic orbits on higher-dimensional tori and has the advantage that it provides a simple algebraic criterion for determining the stability of the orbit, which is directly related to the stability of the fixed point. Hence, it is straightforward to detect quasiperiodic bifurcations (see also [6] and [9]), and an example of a quasiperiodic orbit losing stability is given in [43]. The drawback of this algorithm is that it also suffers from the small divisor problem. Namely, for quasiperiodic orbits with rotation numbers that are well approximated by continued fraction expansion it becomes hard or even impossible to compute the generalised Poincaré map with sufficient precision.

To overcome difficulties caused by properties of the flow on the torus, such as the small divisor problem, research focused on the direct computation of the torus itself or, equivalently, an associated invariant closed curve of a local Poincaré map. In §2.1 we sketch the historical development and the current state of the art of methods for invariant closed curves and tori of maps, and in §2.2 we do the same for tori of ODEs. In the sequel, $\mathbb{T}^p := (\mathbb{R}/2\pi)^p$ denotes the p-dimensional standard torus parametrised over $[0, 2\pi)^p$. A function $u : \mathbb{T}^p \to \mathbb{R}^n$ with domain $\mathbb{T}^p$ is called *torus function*. Note that $\mathbb{T}^1 = S^1$ and that by this definition the 0-torus $\mathbb{T}^0$ is a point, whereas the 0-sphere S^0 consists of two isolated points. For invariant 1-tori of maps and ODEs we also use the terms invariant closed curve and periodic orbit, respectively.

2.1 Tori of Maps

The basic idea is to find a torus function $u : \mathbb{T}^p \to \mathbb{R}^n$ such that its image $T := \{ u(\theta) \mid \theta \in \mathbb{T}^p \}$ is invariant under the map $f : \mathbb{R}^n \to \mathbb{R}^n$. That is, the invariance condition

$$u(\varphi(\theta)) = f(u(\theta)) \tag{2}$$

holds point-wise, where $\theta \in \mathbb{T}^p$ and $\varphi : \mathbb{T}^p \to \mathbb{T}^p$ is diffeomorphic to the map f restricted to the invariant torus T. Here, a typical problem that appears in torus computations becomes visible, namely, the invariance condition (2) provides only an equation for u, but the function φ is also unknown and it depends on the parametrisation of the torus T. One can fix the function φ by either introducing local coordinates or by adding further conditions to (2), a non-trivial task in both cases. Once the function φ is fixed, one transforms (2) into the equivalent fixed point form

$$u(\theta) = f(u(\varphi^{-1}(\theta))), \tag{3}$$

and solves (3), in principle, by fixed-point iteration or by applying Newton's method to one of the problems $u(\varphi(\theta)) - f(u(\theta)) = 0$ or $u(\theta) - f(u(\varphi^{-1}(\theta))) = 0$. We say 'in principle' because we have not specified conditions to fix φ, hence, (2) and (3) are not ready-to-use algorithms.

In 1985 Kevrekidis, Aris, Schmidt and Pelikan [44] published an algorithm for the computation of invariant closed curves based on the invariance condition (2) under the additional assumption that the periodic function u can be parametrised in (global) polar coordinates. In this case, the map f can be transformed into the so-called *partitioned form*, that is, it can be written as

$$f : \begin{pmatrix} r \\ \theta \end{pmatrix} \mapsto \begin{pmatrix} g(r,\theta) \\ h(r,\theta) \end{pmatrix},$$

where $\theta \in S^1$ and $r \in \mathbb{R}$. In other words, f is a map on the cylinder $S^1 \times \mathbb{R}$. Hence, the invariance condition becomes the functional equation $u(h(u(\theta),\theta)) = g(u(\theta),\theta)$ where only $u : S^1 \to \mathbb{R}$ is unknown and which can be solved efficiently with Newton's method. A generalisation of this algorithm to the case of invariant closed curves of general maps in $\mathbb{R}^n$ was proposed by Debraux [18] in 1994. Debraux adds suitable orthogonality conditions to fix the parametrisation. Another method was given in 1996 by Moore [51]. Here, a unique parametrisation is obtained by introducing a local coordinate system.

An algorithm for the computation of invariant closed curves of maps based on the fixed point equation (3) was published in 1987 by Van Veldhuizen [66, 67] where it is assumed that the invariant closed curve can be parametrised by radial coordinates. Therefore, the coordinate system is fixed and it is possible to compute attracting invariant closed curves by iterating the fixed-point equation (3). This algorithm can be regarded as a first implementation of the Hadamard graph transform technique; see also [36].

Dieci and Lorenz [21] proposed in 1995 a generalisation of the graph transform technique to the computation of attracting invariant tori of maps, and examples for 2-tori are given. With the aid of the normal bundle, a local torus-coordinate system is introduced to fix the parametrisation. Therefore, no restrictions on the representation of the map apply. This algorithm allows the computation of the full invariant 2-torus of an ODE when applied to the time-τ map of the flow generated by the ODE. A recent implementation of a continuation method utilising this algorithm includes the re-parametrisation technique described in [51] and can be found in [58].

Independently, in 1996 Broer, Osinga and Vegter [10, 11, 12, 13] developed an algorithm for the computation of invariant tori of maps which is also based on the graph transform technique. This algorithm introduces a local coordinate system utilising the $\partial_x f$-invariant transversal bundle. It is able to compute attracting as well as saddle-type tori and examples of attracting and saddle-type invariant closed curves and 2-tori are given. Furthermore, their algorithm can be used for the computation of compact overflowing invariant manifolds, for instance, local stable and unstable manifolds of compact invariant manifolds. This is demonstrated with examples of the computation of local stable and unstable manifolds of invariant closed curves and invariant 2-tori; these examples appeared in [54].

A further developed version of this algorithm was published in 2003 by Broer, Hagen and Vegter [7]. Here, a Lipschitz-continuous approximation to the normal bundle is used instead of the $\partial_x f$-invariant transversal bundle. This algorithm is implemented on both fixed and adaptive meshes for invariant closed curves and 2-tori. Examples for the computation of attracting as well as saddle-type invariant closed curves and 2-tori of maps and ODEs are given.

In the special case that the restriction of f to the invariant torus T is diffeomorphic to a rigid rotation with rotation vector $\omega \in \mathbb{R}^p$ the invariance condition (2) becomes $u(\theta + \omega) = f(u(\theta))$, that is, $\varphi(\theta) = \theta + \omega$. An algorithm for the computation of invariant tori for this case was published by Castellà and Jorba [15, 39] in 2000. The invariant torus is approximated by truncated Fourier series and the discretised invariance condition is solved by collocation. Additional phase-conditions are introduced to fix the unknown rotation vector ω. If the computed invariant torus is reducible, that is, the normal linear part can be transformed into Floquet form, a stability analysis is possible in terms of the eigenvalues of the Floquet matrix; see [39]. As will become clear in §3, this algorithm can be regarded as the counterpart for maps of the approach proposed in this paper.

2.2 Tori of ODEs

The second main class of algorithms for the computation of invariant tori of ODEs is based on the invariance condition for vector fields. The basic idea is to find a torus function $u : \mathbb{T}^p \to \mathbb{R}^n$ such that its image $T := \{\, u(\theta) \mid \theta \in \mathbb{T}^p \,\}$ is invariant under the flow induced by a vector field. In other words, the vector field restricted to the torus T is everywhere tangent to T. This invariance condition can be rewritten as the first-order partial differential equation (PDE)

$$\sum_{i=1}^{p} \psi_i(\theta) \frac{\partial u}{\partial \theta_i} = f(u)\,, \tag{4}$$

where the $\psi_i : \mathbb{T}^p \to \mathbb{R}$, $i = 1, \ldots, p$, are the coefficients of the vector field restricted to the invariant torus in the base $\{\partial u/\partial\theta_1, \ldots, \partial u/\partial\theta_p\}$. Again, one encounters the problem that (4) provides an equation for u only, while the function ψ is also unknown and depends on the choice of a parametrisation of the torus. As for the computation of invariant tori of maps, the function ψ can be fixed by either introducing local coordinates or by adding further conditions, either of which comes with its own difficulties. Once the function ψ is fixed, one applies Newton's method and obtains a fast-converging algorithm.

An early algorithm that follows this idea was published in 1987 by Samoilenko [61]. It is based on the invariance condition (4) under the additional assumption that the torus function u can be parametrised in (global) torus coordinates. In this case, the ODE can be transformed into the partitioned form

$$\left\{ \begin{array}{rcl} \dot{r} &=& g(r,\theta), \\ \dot{\theta} &=& h(r,\theta), \end{array} \right.$$

where $r \in \mathbb{R}^{n-p}$ and $\theta \in \mathbb{T}^p$. In other words, the ODE is already given in torus coordinates. Hence, the invariance condition (4) assumes the specific form

$$\sum_{i=1}^{p} h_i(u,\theta)\frac{\partial u}{\partial \theta_i} = g(u,\theta)\,, \tag{5}$$

where only the function $u : \mathbb{T}^p \to \mathbb{R}^{n-p}$ is unknown and which can be solved efficiently with Newton's method. Samoilenko considers the computation of quasiperiodic invariant tori by the Fourier-Galerkin method applied to (5) and a thorough convergence analysis of this algorithm is given both in the linear and in the nonlinear case. (He also gives an introduction to the theory of quasiperiodic orbits; the derivation of our invariance equation in §3 is, in fact, based on properties of quasiperiodic orbits stated in [61].)

The numerical approximation of invariant tori independent of the flow on the torus was first considered by Dieci, Lorenz and Russell [19] in 1991. Equation (5) is discretised by a finite difference method and a proof of convergence is given in [20]. Other discretisation methods for equation (5) were also studied; see, for example, [4, 25, 29, 50]. The performance of these algorithms is demonstrated with examples for the computation of attracting invariant 2-tori. An extension to the computation of invariant 2-tori of ODEs that cannot be transformed into radius-angle coordinates was published by Moore [51] in 1996. Moore introduces a local coordinate system around the torus and, thereby, fixes the unknown function ψ. He also addresses the problem that a suitable initial parametrisation may become inappropriate during a parameter continuation and develops a re-parametrisation technique which produces parametrisations of high quality.

For Hamiltonian systems there exist further approaches that are not based on invariance conditions; see, for example, [16, 28, 38, 40, 47]. One possibility is to compute integrable normal form approximations to a given vector field [28, 38]. Then, the families of invariant tori can be given explicitly. Another method is to implement the Poincaré-Lindstedt perturbation method in the way it is used to prove existence of quasiperiodic invariant tori [40]. Note that this method can also be applied to some dissipative systems, for example, weakly coupled oscillators. Both methods are 'semi-analytical', that is, they are implemented using algebraic manipulators. These algorithms were used to compute families of invariant tori in a Hamiltonian setting near (elliptic) equilibria for fixed-parameter vector fields. Since these approaches are local by nature, restricted to Hamiltonian systems or not suited for use in predictor-corrector continuation environments, we do not discuss these methods here.

2.3 Comparison

The two main approaches for the computation of invariant tori of maps and ODEs, namely, applying Newton's method to a functional equation and the graph transform technique, have inherent strengths and weaknesses. The functional equation approach has the advantage that one obtains quadratically convergent algorithms by employing Newton's method, whereas algorithms based on the graph transform technique are only linearly convergent. Furthermore, the speed of convergence of Newton's method is independent of the properties of the flow near the torus while the speed of convergence of the graph transform technique is determined by the attraction (expansion) transverse to the torus. In particular, during a parameter continuation, algorithms based on the graph transform technique cannot 'step over' small parameter intervals where the torus changes stability.

On the other hand, the graph transform technique is memory conservative. It requires only to store the mesh and can be implemented to work node by node.

Thus, it is not necessary to have simultaneous access to the full stored data. In contrast, for applying Newton's method it is necessary to store not only the mesh but also a Jacobian and its (incomplete) factorisation. Therefore, compared with Newton's method, the graph transform technique allows the computation of higher-dimensional tori under the restriction of sufficient normal attraction (expansion).

A complete proof of convergence for normally hyperbolic invariant tori is only available for algorithms based on the graph transform. In fact, these algorithms can be regarded as implementations of the constructive proof of existence given in [36]. Convergence of Newton's method was investigated in two special cases. First, the existence of invariant tori for which the restricted flow (map) is equivalent to a parallel flow (rigid rotation) with the same frequency basis (rotation vector) is the principal object of the (dissipative) KAM theory; for recent overviews see [8, 48]. Constructive proofs of existence are based on the Poincaré-Lindstedt perturbation method and the hard implicit function theorem. Typically, existence of fast converging Fourier series can be established under some assumptions on the frequency basis and the normal behaviour of the vector field (map). The application of the hard implicit function theorem gives convergence of Newton's method using Fourier approximations as a by-product. Thus, the approximation of quasiperiodic invariant tori of maps, as described at the end of §2.1, can be regarded as an implementation of such a proof.

Secondly, for algorithms using the invariance condition (5) convergence can be established under strong assumptions on the vector field. The major difficulty here is to show stability of the discretisation. Such a proof of stability is given by Dieci and Lorenz [20] for a finite-difference scheme.

A problem that both main approaches share is the choice of a suitable parametrisation, which is non-trivial as we already pointed out. This is the major difficulty for the construction of algorithms that are simple to implement. Our main goal is to overcome this difficulty. As a first step we derive a PDE that gives rise to a parametrisation of quasiperiodic invariant tori in a natural way. The discretisation of this equation provides an algorithm that not only computes a quasiperiodic invariant torus but also its basic frequencies. The method is simple to implement, uses only information in the tangent space and can be regarded as a natural generalisation of algorithms for periodic orbits. Furthermore, it is used in a multi- as well as a one-parameter continuation environment where, in the latter, it is capable of computing phase-locked tori, provided the resonances are 'sufficiently weak' relative to the used mesh; see §4.3.

3 Invariance Equation

In this section we derive an extended PDE that an invariant quasiperiodic torus must satisfy. We represent an invariant torus by a torus function $u : \mathbb{T}^p \to \mathbb{R}^n$ with the p-dimensional standard torus $\mathbb{T}^p := (\mathbb{R}/2\pi)^p$ parametrised over $[0, 2\pi)^p$ as its domain. The general invariance condition is then the first order PDE

$$\sum_{i=1}^{p} \psi_i(\theta) \frac{\partial u}{\partial \theta_i} = f(u)\,,$$

where the $\psi_i : \mathbb{T}^p \to \mathbb{R}$, $i = 1, \ldots, p$, are the coefficients of the vector field restricted to the invariant torus in the base $\{\partial u/\partial\theta_1, \ldots, \partial u/\partial\theta_p\}$. Instead of transforming this equation into (local) torus coordinates to fix the functions ψ_i, we propose to choose a *canonical form* for the unknown functions ψ_i, thereby implicitly defining a coordinate system on the torus. For an invariant torus with parallel flow, such a canonical form is well known and given by $\psi_i \equiv \omega_i = \text{constant}$. In fact, this is the

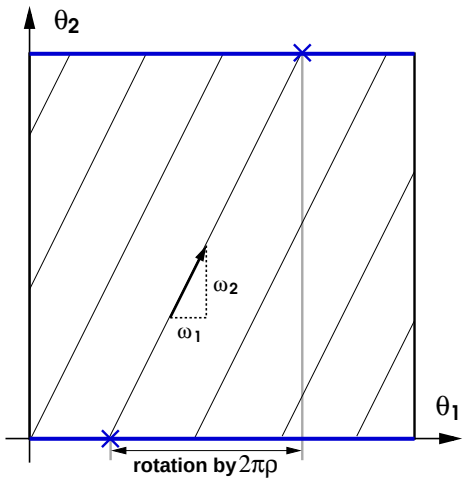

Figure 1: The characteristic field of equation (6) on the standard torus $\mathbb{T}^2$ is a set of parallel straight lines with slope $\varrho = \omega_2/\omega_1$. The cross-section $\theta_2 = 0$ (blue lines) is mapped onto itself under the transport along the characteristics whereby a rotation by $2\pi/\varrho$ occurs.

normal form of a parallel flow on a torus with *basic frequencies* ω_i, $i = 1, \ldots, p$, and $\omega = (\omega_1, \ldots, \omega_p)$ is called the *frequency basis*. This choice leads to the specific PDE

$$\sum_{i=1}^{p} \omega_i \frac{\partial u}{\partial \theta_i} = f(u) \tag{6}$$

and the invariant torus T is given by $T := \{\, u^*(\theta) \mid \theta \in \mathbb{T}^p \,\}$, where $u^* : \mathbb{T}^p \to \mathbb{R}^n$ is a solution of (6). As yet, no canonical form is known for families of invariant tori with both quasiperiodic and phase-locked flow. It is not even clear, if such a canonical form would depend on finitely or infinitely many parameters.

Equation (6) has some remarkable properties that are closely related to the properties of the flow on the torus; see Fig. 1:

1. The characteristic field is a set of parallel straight lines.
2. A solution u^* maps the characteristic field onto the flow on T.
3. The sections $\theta_i = 0$ are invariant under the period-$2\pi/\omega_i$ stroboscopic maps.
4. Equation (6) is a direct generalisation of the equations for equilibrium points ($p = 0$) and periodic orbits ($p = 1$).

For these reasons, we call a parametrisation of T generated by a solution of equation (6) a *natural parametrisation* of the torus T.

3.1 Phase conditions

Similar to periodic orbits, an invariant quasiperiodic torus of (1) is not uniquely defined by the partial differential equation (6). For any quasiperiodic invariant p-torus, both the torus function u and the frequency basis ω are unknown but (6) is an equation for the torus function only. This is due to the fact that the p-torus T has p *free phases*. In order to fix the free phases and allow the computation of the basis frequencies we introduce *phase conditions* as follows.

Assume that we already know a nearby solution $\tilde{u}$, for instance from a previous continuation step. Then we take $s \in \mathbb{T}^p$ such that the parametrisation $u(\theta + s)$ is an extremal point of the function $g(s) := \|\tilde{u} - u\|^2$ in some suitable norm. Here, we implicitly define the parametrisation $u^*(\theta) := u(\theta + s^*)$ by the necessary conditions of extremality of $g(s^*)$ with respect to the $\mathcal{L}_2$-norm, namely,

$$\left\langle \frac{\partial \tilde{u}}{\partial \theta_i} \, , \, u \right\rangle := \frac{1}{(2\pi)^p} \sum_{j=1}^{n} \int_{\mathbb{T}^p} \frac{\partial \tilde{u}_j}{\partial \theta_i}(\theta) \, u_j(\theta) \, d\theta = 0 \, , \qquad i = 1, \ldots, p \, .$$

This idea generalises the phase condition used in AUTO [23] and in [24] for the computation of periodic orbits. By adding these phase conditions to equation (6) we obtain the extended system

$$\left\{ \begin{array}{rcl} \displaystyle\sum_{i=1}^{p} \omega_i \frac{\partial u}{\partial \theta_i} & = & f(u) \, , \\ \\ \left\langle \dfrac{\partial \tilde{u}}{\partial \theta_i} \, , \, u \right\rangle & = & 0 \, , \qquad i = 1, \ldots, p \, , \end{array} \right. \tag{7}$$

which has as many equations as unknowns and where $\tilde{u}$ is an a-priori known initial approximation. We refer to system (7) as the *invariance equation*.

3.2 Existence

As mentioned above, a solution u^* of equation (6) provides a diffeomorphism of the quasiperiodic flow on the invariant torus with a parallel flow on the standard torus having the same frequency base. Furthermore, if such a diffeomorphism exists then it is a solution of (6) and vice versa. The existence of diffeomorphisms with the above properties is the principal object of the dissipative KAM theory. Under certain conditions, involving number theoretical properties of the frequency basis, existence can be shown; for recent overviews we refer to [6, 8, 9, 48]. Qualitatively, for systems depending on at least p parameters $\lambda \in \mathbb{R}^m$, $m \geq p$, such that the Jacobian of $\omega(\lambda)$ has full rank for parameter values in some open connected set $\lambda \in \Omega \subseteq \mathbb{R}^m$, a main result is that quasiperiodic invariant tori can exist for parameter values in smooth manifolds of codimension $p-1$, the flow on these tori being equivalent, that is, the rotation vector $\varrho = (\omega_2/\omega_1, \ldots, \omega_p/\omega_1)$ is constant. The union of these manifolds is nowhere dense in the parameter space, however, it has positive measure [6, 8, 9]. See §4.3 for typical settings for which quasiperiodic invariant tori exist.

Note that existence of quasiperiodic tori does not automatically imply well-posedness of the invariance equation (7). By differentiating (6) with respect to θ_i, $i = 1, \ldots, p$, it is straightforward to show that p phase conditions, such as in (7), are necessary for solvability, but a proof that these are also sufficient presents great technical difficulties, even under strong assumptions; see also §4.1.

4 Numerical Approximation

In this section we describe the computation of approximate solutions of the invariance equation (7). To this end, we introduce appropriate mesh-functions and approximate the partial derivatives by central difference quotients; see §4.1. Because of the specific structure of the invariance equation (7) the discretised system can be constructed recursively, whereby the dimension p of the torus is used as the recursion parameter; see §4.2. This already reduces the implementation effort in the case of 2-tori and means that our implementation is able to compute invariant

tori of arbitrary fixed dimension p. In §4.3 we explain how to integrate this method in a continuation algorithm. Here, we also address convergence problems that may occur during a one-parameter continuation since quasiperiodic invariant tori do not persist under generic perturbations.

4.1 Discretisation by Finite Differences

A discretisation of equation (7) by finite differences seems especially advantageous because the domain $\mathbb{T}^p$ is compact and has no boundary. We choose p arbitrary but fixed natural numbers $N_1, \ldots, N_p$ and call $N := \min\{N_1, \ldots, N_p\}$ the *discretisation parameter*. We define the *step-sizes* $h_i := 2\pi/N_i$, $i = 1, \ldots, p$, and call $h := \max\{h_1, \ldots, h_p\} = 2\pi/N$ the *mesh size*. The mesh points are now defined using the one-dimensional toroidal index-sets $\mathbb{T}_{N_i} := \mathbb{Z}/N_i$, $i = 1, \ldots, p$, and $\mathbb{T}_N^p := (\mathbb{T}_{N_1}) \times \cdots \times (\mathbb{T}_{N_p})$ is the corresponding p-dimensional toroidal multi-index set. The mesh-functions are defined on the space $\mathbb{G}_N := \{\, u_N \mid u_N : \mathbb{T}_N^p \to \mathbb{R} \,\}$. A mesh-function on $\mathbb{T}_N^p$ is indicated by the sub-index N. Addition of two mesh-functions and multiplication with a scalar are defined point-wise. In the space of vector-valued mesh functions $[\, \mathbb{G}_N \,]^n$ we define a scalar product

$$\langle\, u_N \,,\, v_N \,\rangle_{[\, \mathbb{G}_N \,]^n} \;:=\; \sum_{i=1}^{n} \langle\, u_{N,i} \,,\, v_{N,i} \,\rangle_{\mathbb{G}_N} \,, \tag{8}$$

$$\langle\, u_{N,i} \,,\, v_{N,i} \,\rangle_{\mathbb{G}_N} \;:=\; \frac{1}{N_1 \cdots N_p} \sum_{j \in \mathbb{T}_N^p} u_{N,i}(j) v_{N,i}(j) \,, \tag{9}$$

and use the induced norm.

We now discretise the invariance equation (7) by restricting to functions defined only on the mesh points $\mathbb{T}_N^p$. We denote this discretisation in terms of the discretisation operator $P_N : [\, \mathcal{C}^r(\mathbb{T}^p) \,]^n \to [\, \mathbb{G}_N \,]^n$, $(P_N u)(j_1, \ldots, j_p) := u(j_1 h_1, \ldots, j_p h_p)$, sometimes also referred to as the restriction operator. Furthermore, we approximate the partial differential operators by the partial finite-difference operators $\partial_{N,i} : [\, \mathbb{G}_N \,]^n \to [\, \mathbb{G}_N \,]^n$,

$$\partial_{N,i} u_N := \frac{1}{h_i} \sum_{k=-m}^{m} \eta_k u_N(\ldots, j_i + k, \ldots) \,, \qquad \eta_k \in \mathbb{R} \,,\;\; i = 1, \ldots, p \,,$$

where we use central finite-difference quotients for which the coefficients η_k are skew symmetric, that is, $\eta_k = -\eta_{-k}$ for $k = 0, \ldots, m$. In our implementation we use the finite-difference quotients for $m = 1$, $\eta_1 = 1/2$, of order 2 and for $m = 2$, $\eta_1 = 8/12$, $\eta_2 = -1/12$, of order 4, respectively, and compute two solutions on the same mesh. Thus, we estimate the approximation error as the norm of the difference between these two solutions.

We introduce a compact notation for this discretisation by using the difference operator $D_N : [\, \mathbb{G}_N \,]^n \to [\, \mathbb{G}_N \,]^n$, $D_N u_n := \sum_{i=1}^{p} \omega_i \partial_{N,i} u_N$, and define for brevity

$$f_N(u_N)(j_1, \ldots, j_p) \;:=\; P_N(\, f(u(\theta)) \,)(j_1, \ldots, j_p) \;=\; f(u(j_1 h_1, \ldots, j_p h_p)) \,.$$

With these definitions the discretised invariance equation (7) is given by

$$\left\{ \begin{array}{rcll} D_N u_N & = & f_N(u_N) \,, & \\ \langle\, \partial_{N,i} P_N \tilde{u} \,,\, u_N \,\rangle & = & 0 \,, & i = 1, \ldots, p \,. \end{array} \right. \tag{10}$$

We solve system (10) by applying Newton's method. To this end, it is convenient to rewrite (10) as the root-finding problem

$$F_N(u_N, \omega) := \left(\begin{array}{c} f_N(u_N) - D_N u_N \\ \langle\, \partial_{N,i} P_N \tilde{u} \,,\, u_N \,\rangle \end{array} \right) = 0 \,, \tag{11}$$

where $F_N : ([\,\mathbb{G}_N\,]^n \times \mathbb{R}^p) \to ([\,\mathbb{G}_N\,]^n \times \mathbb{R}^p)$. Note that the dependence of F_N on ω is due to the dependence of D_N on ω which, for simplicity, is not explicitly noted.

Our method can also be used in the case that forcing is present, that is, (1) has the form

$$\dot{x} = f(x, \omega_1 t, \ldots, \omega_q t, \lambda),$$

where $q \leq p$ is the number of forcing frequencies. One way to do this, is to extend this system by a nonlinear harmonic oscillator for each forcing frequency and apply the algorithm as described; this technique is also used in AUTO [23]. An other possibility, which we followed in our implementation, is to drop the corresponding phase conditions and use additional time-like arguments. This results in much smaller linear equation systems at the expense of a slightly more involved implementation.

For our finite-difference discretisation, convergence can be shown under strong assumptions on the right-hand side f of the ODE (1), the proof of stability being valid only in the special case that system (1) is quasiperiodically forced, that is, $q = p$. Although an abstract well-posedness and stability result holds for (7) and (11), there is the problem that, as yet, no pointwise conditions on the Jacobian of f are known that imply its requirements in general; see [62].

4.2 Recursive Construction of the Discretised System

When developing numerical algorithms on multi-dimensional domains one typically introduces a bijective map of the set of multi-indices onto a set of single indices such that the discrete function values can be stored as vectors. Thereby, one obtains a finite-dimensional nonlinear algebraic system. In the following, we present a different approach that not only simplifies the implementation but also allows the computation of tori of arbitrary dimension $p \geq 1$.

Consider the PDE (6) for tori of dimension $p \geq 0$ written as a root-finding problem in function space:

$$0 = F^p(u) := \left(f(u) - \sum_{i=1}^{p-1} \omega_i \frac{\partial u}{\partial \theta_i} \right) - \omega_p \frac{\partial u}{\partial \theta_p} = F^{p-1}(u) - \omega_p \frac{\partial u}{\partial \theta_p}\,.$$

We observe that the expressions on the right-hand side can be formed recursively. This motivates the idea of developing an algorithm that constructs the extended discrete system (10) by recursion over the dimension p of the torus.

Let $p \geq 1$ and natural numbers $N_1, \ldots, N_p$ be given. Similar to §4.1 we define the discretisation parameter N, the step-sizes h_i, the mesh-size h and the toroidal index-sets $\mathbb{T}_{N_i}$, $i = 1, \ldots, p$. This time, we recursively define the spaces of mesh-functions:

$$\begin{aligned} \mathbb{G}_N^1 &:= \{\, u_N^1 \mid u_N^1 : \mathbb{T}_{N_1}^1 \to \mathbb{R} \,\}\,, \\ \mathbb{G}_N^q &:= \{\, u_N^q \mid u_N^q : \mathbb{T}_{N_q}^1 \to \mathbb{G}_N^{q-1} \,\}\,, \end{aligned}$$

where $q = 2, \ldots, p$ is the recursion parameter. In the space of vector-valued recursive mesh functions $[\,\mathbb{G}_N^q\,]^n$ we define a scalar product

$$\begin{aligned} \langle\, u_N^q \,,\, v_N^q \,\rangle_{[\,\mathbb{G}_N^q\,]^n} &:= \sum_{i=1}^{n} \left\langle\, u_{N,i}^q \,,\, v_{N,i}^q \,\right\rangle_{\mathbb{G}_N^q}\,, \\ \left\langle\, u_{N,i}^q \,,\, v_{N,i}^q \,\right\rangle_{\mathbb{G}_N^q} &:= \frac{1}{N_q} \sum_{j=1}^{N_q} u_{N,i}^q(j) v_{N,i}^q(j)\,, \end{aligned}$$

and use its induced norm. Addition of two mesh-functions and multiplication with a scalar are defined recursively point-wise. The discretisation operator $P_N : [\,\mathcal{C}^r(\mathbb{T}^p)\,]^n \to [\,\mathbb{G}_N^p\,]^n$ now assumes the form $(P_N u)(j_1)\dots(j_p) := u(j_1 h_1, \dots, j_p h_p)$. If we identify $u_N(j_1,\dots,j_p)$ and $u_N^p(j_1)\dots(j_p)$ then the spaces $[\,\mathbb{G}_N\,]^n$ and $[\,\mathbb{G}_N^p\,]^n$ are isometric.

One can interpret a mesh-function $u_N^q \in [\,\mathbb{G}_N^q\,]^n$ as a q-dimensional array with elements in $\mathbb{R}^n$. The recursive definition is yet another way to actually perform the index computation and the notation $u_N^q(j_1)\dots(j_q)$ is closely related to the recursive indexing of arrays in C and C++. Its main advantage is that an element $u_N^q \in [\mathbb{G}_N^q]^n$ can be regarded as an object with an index map that has to be defined for one-dimensional indices only, for instance, by operator overloading. Thus, the dimension p of the torus becomes a free parameter in our algorithm and we implemented the mesh-functions $u_N^q \in [\,\mathbb{G}_N^q\,]^n$ as a template-class with q as a template-parameter.

With the above definitions, a recursive algorithm for the evaluation of F_N in (11) is given by

$$F_N^p(u_N^p,\omega) := \begin{pmatrix} G_N^p(u_N^p,\omega) \\ b_N^p(u_N^p) \end{pmatrix}, \tag{12}$$

where G_N^q contains the recursive discretisation of the PDE (6) :

$$G_N^q(u_N^q,\omega)(j) := \begin{cases} f(u_N^1(j)) - \omega_1(\partial_{N,1}u_N^1)(j) & \text{for} \quad q = 1\,, \\ G_N^{q-1}(u_N^q(j),\omega) - \omega_q(\partial_{N,q}u_N^q)(j) & \text{for} \quad q > 1\,, \end{cases} \tag{13}$$

the term b_N^p represents the discretised phase conditions:

$$b_N^p(u_N^p) := \begin{pmatrix} \langle\, \partial_{N,1}\, \tilde{u}_N^p\,,\, u_N^p \,\rangle \\ \vdots \\ \langle\, \partial_{N,p}\, \tilde{u}_N^p\,,\, u_N^p \,\rangle \end{pmatrix}, \tag{14}$$

and the finite-differences $\partial_{N,i}$ are recursively evaluated according to:

$$(\partial_{N,i}u_N^q)(j) := \begin{cases} \dfrac{1}{h_q}\displaystyle\sum_{k=1}^{m} \eta_k\,(\,u_N^q(j+k) - u_N^q(j-k)\,) & \text{for} \quad i = q\,, \\ \partial_{N,i}u_N^q(j) & \text{for} \quad i < q\,. \end{cases} \tag{15}$$

This algorithm not only has the advantage that the dimension p of the torus is a free parameter, but the finite-difference formula also appears only in its one-dimensional form at label $i = q$ of (15). This remarkably simplifies the implementation of a particular finite-difference scheme as well as its substitution by another one.

One obtains a recursive algorithm for the evaluation of the Jacobian $(F_N^p)'$ by differentiating (12-15). Fig. 2 shows the structure-plot of a Jacobian of the system of two coupled Van der Pol oscillators described in §5.1, illustrating the typical bordered, recursive block-structure. The diagonal blocks are occupied by the Jacobians of the right-hand side f evaluated at the mesh points. The off-diagonal blocks contain the coefficients of the finite-difference operators $\partial_{N,i}$. Without the diagonal blocks, these matrices are skew-symmetric due to the use of central finite-difference quotients. Hence, these Jacobians are in general indefinite and one has to use linear equation solvers for general systems. In the present implementation of our algorithm, we solve these systems using GMRES together with an ILU preconditioner, both provided by the software package SPARSKIT [60]. The preconditioner was slightly modified to deal more effectively with bordered systems.

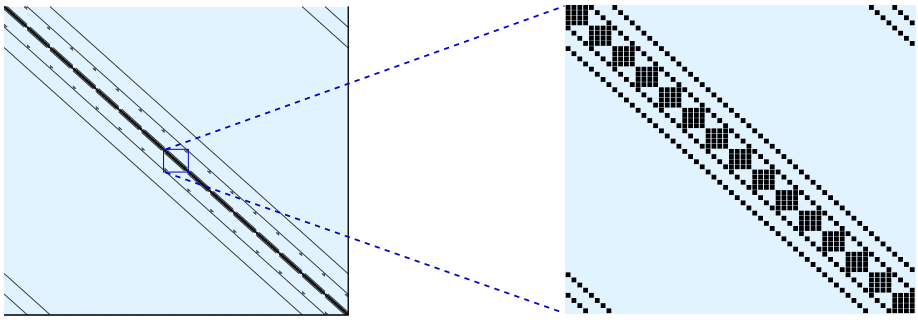

Figure 2: Typical structure of the Jacobian $(F_N^2)'$, the black squares indicate the positions of structural non-zero elements. The structure of the matrix repeats recursively block-wise as indicated. The diagonal blocks contain the Jacobians of the right-hand side f at the mesh points and the off-diagonal blocks the coefficients of the finite-difference formula.

4.3 Continuation

We implemented the proposed method as a corrector in pseudo-arclength continuation algorithms [59]. We consider two cases, the continuation with respect to p parameters, which is well-defined as explained in §3.2, and the continuation with respect to one parameter, which demands further discussion. Consider a typical situation as sketched in Fig. 3 (a). Let us assume that for $\varepsilon = 0$ a family of normally hyperbolic invariant 2-tori with parallel flow exists and that the rotation number $\varrho = \omega_2/\omega_1$ varies with μ, that is, $|d\varrho/d\mu| \geq \delta > 0$. This is satisfied, for example, for a system of two coupled nonlinear oscillators, each of which possessing a hyperbolic periodic orbit. Then, for small $\varepsilon \neq 0$ and each μ such that $\varrho(\mu)$ satisfies certain number-theoretical conditions, there are curves in (μ, ε)-space (Fig. 3 (a), label 1) along which quasiperiodic invariant tori exist such that the rotation number is constant along these curves; see [2, 6, 8, 9, 30, 32] for more details. This 2-parameter continuation setting was used for the example in §5.1.

Independent of μ, the tori persist as differentiable manifolds due to normal hyperbolicity, but the flow on the tori typically changes from parallel to phase-locked [27, 36, 68]. The parameter space features so-called Arnol′d or resonance tongues, sketched as shaded areas in Fig. 3 (a). During a one-parameter continuation, as indicated by the black line (label 2) in Fig. 3 (a), the parameter curve will cross Arnol′d tongues. Since the invariance equation (7) does not hold for phase-locked tori we cannot expect convergence in a strict sense. On the other hand, the set of parameter values for which the flow on the tori is quasiperiodic has positive measure, hence, there is a positive probability to find a quasiperiodic torus. Furthermore, any actual discretisation is of finite accuracy only. Therefore, we can expect that the algorithm also computes approximations to phase-locked tori, provided the resonance is 'weak enough'.

The terms *weaker resonance*, *stronger resonance* and *weak enough resonance* are used in the following sense. We introduce an ordering of p:q resonances in terms of the period of the occurring periodic orbits, which is essentially proportional to the denominator q. A resonance is called weaker, if this period is greater than that of another resonance, and stronger otherwise, that is, the greater q the weaker the resonance. The resonances with $q \in \{1, 2, 3, 4\}$ play a special role and are called *strong resonances*; see, for example, [32]. If the period of a resonance is so high that the flow on the torus can be regarded as parallel within the accuracy of a particular discretisation, we call the resonance weak enough.

Within a one-parameter continuation method we expect our algorithm to be-

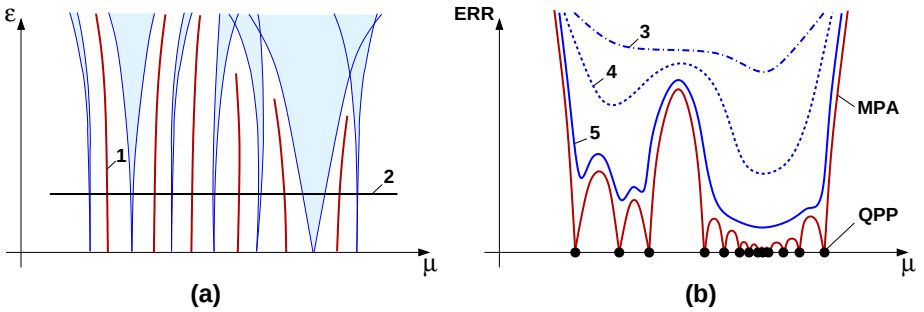

Figure 3: Sketch of Arnol′d tongues in a two-dimensional parameter space (a). In between the Arnol′d tongues exist continuous curves (red, label 1), where the flow on the torus is quasiperiodic. Panel (b) shows a sketch of the expected convergence behaviour of our algorithm during a one-parameter continuation as indicated by the black horizontal line (label 2) in panel (a). For increasing but fixed discretisation parameter N we expect the estimated error ERR that depends on the parameter μ to behave qualitatively similar to the blue lines in the sequence 3-4-5. The points QPP on the μ-axis mark the parameter values where the torus is quasiperiodic. The maximal possible accuracy of our algorithm is drawn as the red curve MPA.

have qualitatively as depicted in Fig. 3 (b). Suppose that the flow on the torus is quasiperiodic for the parameter values μ marked by the points QPP. Then, the red curve MPA sketches the maximal possible accuracy that our algorithm can reach theoretically when the flow on the torus is not parallel. The blue lines with labels 3, 4 and 5 illustrate an actual accuracy for discretisations with discretisation parameters $0 < N_1 < N_2 < N_3$, respectively. An estimate of this accuracy must be monitored during continuation. As long as the encountered resonances are weak enough, our algorithm will compute a solution within its prespecified numerical accuracy. For μ-values that belong to stronger resonances the actual accuracy of the obtained mesh function will not improve as the mesh is refined. Thus, we expect peaks in the approximation error due to stronger resonances, the height of which indicates the 'strength' of a resonance. For all other parameter values we expect to observe convergence. When the parameter value gets close to a region where the torus is strongly resonant, the algorithm will eventually break down. After passing through an Arnol′d tongue the algorithm is expected to resume the computation of apparently smooth mesh functions.

5 Examples

In this section we demonstrate the performance of our algorithm with three examples. First, in §5.1, we continue quasiperiodic invariant 2-tori of the system of two coupled Van der Pol oscillators with respect to two external parameters and different but fixed irrational rotation numbers $\varrho = \omega_2/\omega_1$. This example shows that, when considering the computation of 2-tori as a two-parameter problem, our algorithm works stably and provides a good overview about the geometry of the occurring tori. In the second and third example, we 'misuse' our algorithm for one-parameter continuations of invariant 2-tori. The second example, a parametrically forced network of Philippow [57] discussed in §5.2, is particularly difficult for our algorithm, because strong resonances with wide Arnol′d tongues exist in two-parameter space. Our last example described in §5.3 can be regarded as a typical area of application of our algorithm in a one-parameter continuation. The two basic frequencies are of different order of magnitude, so that strong resonances are not

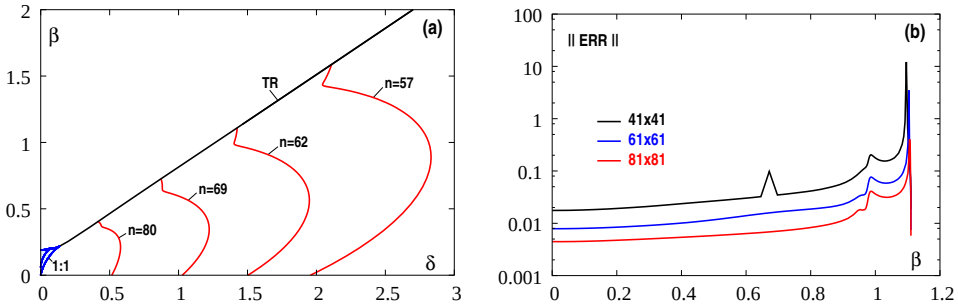

Figure 4: Bifurcation diagram for system (16) of two coupled Van der Pol oscillators in the (δ, β) parameter plane (a). The 1:1 resonance tongue is the shaded area in the bottom-left corner and for parameter values on the red curves the flow on the tori is quasiperiodic with fixed rotation number $\varrho = n\sqrt{2}/140 \approx n/100$ as indicated. For increasing β the tori collapse in a Neimark-Sacker or torus bifurcation (curve TR). Panel (b) shows the estimated error for rotation number $\varrho = 62\sqrt{2}/140$ measured via the parameter β for different meshes, illustrating the typical convergence behaviour during a two-parameter continuation.

expected to occur. The invariant tori undergo 'local bifurcations' (see §5.3) and our algorithm has no problems to 'step over' the regions where the tori change stability, as well as to compute the parts of the branches where the tori are of saddle type.

5.1 Two Coupled Van der Pol Oscillators

As our first example we continue quasiperiodic invariant tori of the system of two coupled Van der Pol oscillators

$$\left\{ \begin{array}{rcl} \ddot{x} + \varepsilon(x^2 - 1)\dot{x} + x & = & \beta(y - x), \\ \ddot{y} + \varepsilon(y^2 - 1)\dot{y} + (1 + \delta)y & = & \beta(x - y). \end{array} \right. \tag{16}$$

Here, ε controls the non-linearity, β is the coupling and δ the detuning parameter that controls the natural frequency of the second oscillator. Since this system is frequently discussed in dynamical systems literature (for example in [29, 32, 56]), we use it here as a test example rather than providing a more thorough analysis. For $\beta = 0$ the system decouples and each of the oscillators has a limit cycle for $\varepsilon, \delta > 0$ [32]. Thus, system (16) has, for $\beta = 0$, a family of normally attracting invariant tori with parallel flow. Note that the rotation number $\varrho = \omega_2/\omega_1$ depends regularly on δ. Hence, for fixed $\varepsilon > 0$ there exist curves in the (δ, β) parameter space for which the tori have fixed irrational rotation number.

For our subsequent continuation with respect to the parameters δ and β, we fixed $\varepsilon = 0.5$. As a seed solution we used the torus function

$$\{\, x(\theta) = 2\sin\theta_1,\ \ \dot{x}(\theta) = 2\cos\theta_1,\ \ y(\theta) = 2\sin\theta_2,\ \ \dot{y}(\theta) = 2.19\cos\theta_2 \,\}$$

together with the basic frequency $\omega_1 = 1$ and the rotation numbers $\varrho = n\sqrt{2}/140 \approx n/100$, with $n = 80, 69, 62, 57$, respectively. Note that algebraic irrationals are Diophantine [48]. We computed and continued approximations of the tori for each rotation number on 41×41, 61×61 and 81×81 meshes. Fig. 4 (a) shows the bifurcation diagram in the (δ, β) parameter plane. The computed curves (red, labelled according to the rotation number) start at the line $\beta = 0$ and end at a locus of Neimark-Sacker or torus bifurcations, which, as well as the boundary of the 1:1 resonance tongue, was computed using AUTO [23]. If one would compute more and more such curves of tori, one could sweep large regions of parameter space and obtain a more and more complete picture.

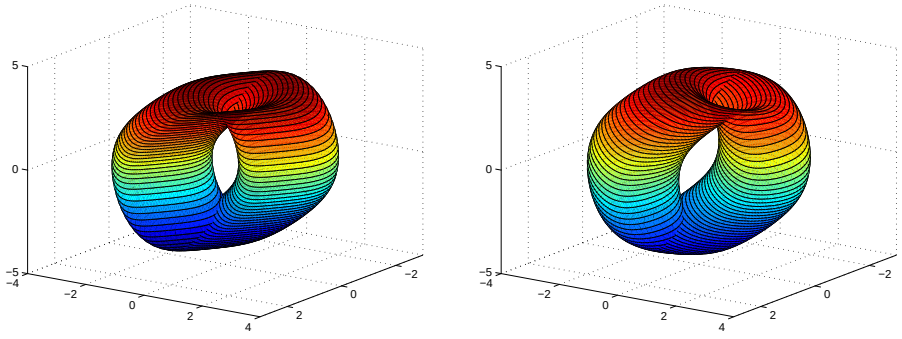

$\beta = 0.000$, $\delta = 1.503$

$\beta = 0.340$, $\delta = 1.873$

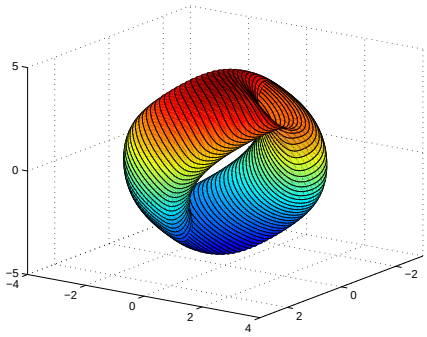

$\beta = 0.838$, $\delta = 1.782$

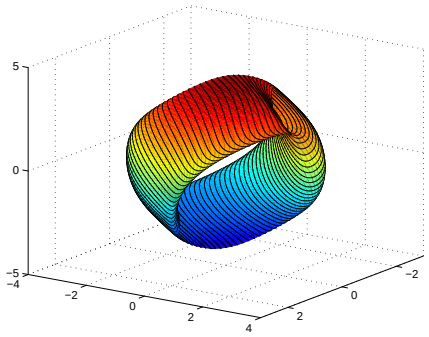

$\beta = 0.984$, $\delta = 1.408$

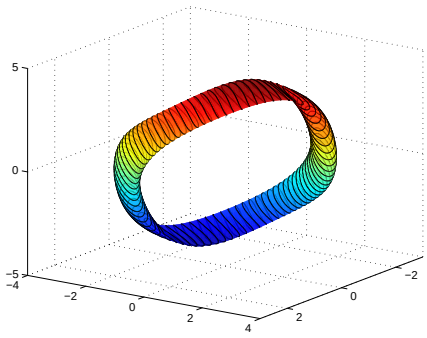

$\beta = 1.079$, $\delta = 1.422$

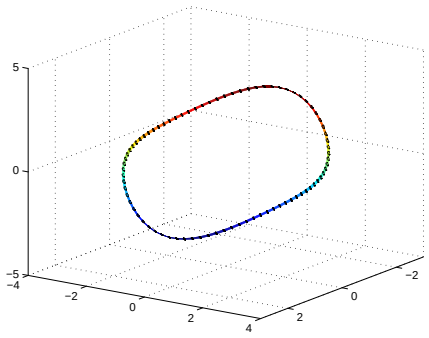

$\beta = 1.110$, $\delta = 1.425$

Figure 5: Invariant tori of system (16) of two coupled Van der Pol oscillators for different values β and δ such that the rotation number $\rho = 62\sqrt{2}/140$. For $\beta = 0$ the system is decoupled and for increasing $\beta > 0$ an inverse torus bifurcation is observed. The tori are projected onto the subspace orthogonal to $(1, 1, 1, 0)^{\mathrm{T}}$; the self-intersection is due to this projection.

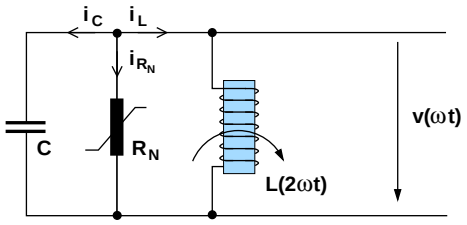

Figure 6: A parametrically forced network with a non-linear resistor and a time-dependent inductor as modelled by equation (17). The characteristic of the resistor is approximately cubic and has regions with negative slope. The periodic forcing is due to the time-dependence of the inductance.

The typical convergence behaviour of our method during a two-parameter continuation is depicted in Fig. 4 (b) for $n = 62$ ($\varrho \approx 0.626$). The estimated error is shown as a function of β for the above meshes; see §4.1 for how the error is measured. For small values of β, where we have shown existence, the data clearly indicates convergence. Close to the torus-bifurcation point on this branch at $\beta \approx 1.11$ we observe large errors, which are due to the 'loss of one dimension' of the torus. Namely, an inverse torus bifurcation occurs and the torus collapses into a periodic orbit. As a result, our discretised system for a 2-torus becomes more and more ill-conditioned as we approach the bifurcation point. Fig. 5 shows some of the tori along this branch. The tori look virtually the same for the other branches and also the estimated error behaves very similar.

5.2 A Parametrically Forced Electrical Network

As our second example we investigate a nonlinear network arising in electrical engineering, given by Philippow in [57] and used as a 2:1 frequency divider. The circuit is depicted in Fig. 6 and its model equation can be derived as follows. Since it is a shunt circuit the drop of voltage over each element is identical and we denote it by $v(\omega t)$. Applying Kirchhoff's laws we obtain a differential equation from the node equation

$$i_C + i_{R_N} + i_L = 0$$

where the currents i_C, i_{R_N} and i_L, respectively, are given by the formulas

$$\begin{aligned} i_C &= C\frac{dv}{dt}\,, \\ i_{R_N} &= b_1 v^3 - b_2 v\,, \\ i_L &= \frac{\psi}{L_0(1+\frac{b}{2}\sin 2\omega t)} \approx \frac{\psi}{L_0}\left(1 - \frac{b}{2}\sin 2\omega t\right)\,. \end{aligned}$$

Using the relation $v = \frac{d\psi}{dt}$ for the inductance and denormalising all quantities one can derive an ODE of the form; see [57],

$$\ddot{x} + \alpha\dot{x}^3 - \beta\dot{x} + (1 + B\sin 2t)x = 0. \tag{17}$$

Here, $x \in \mathbb{R}$ is the normalised voltage and the parameters $\alpha = \varepsilon - B$ and $\beta = \frac{\varepsilon}{2} - B$, where $B, \varepsilon \in \mathbb{R}$, are chosen such that the system response $x(t)$ is an almost harmonic 2π-periodic signal, in other words, the frequency of the input signal is halved.

5.2.1 Qualitative Analysis

In what follows we investigate the qualitative behaviour of solutions of equation (17) over a wide range of parameter values and demonstrate the existence of invariant

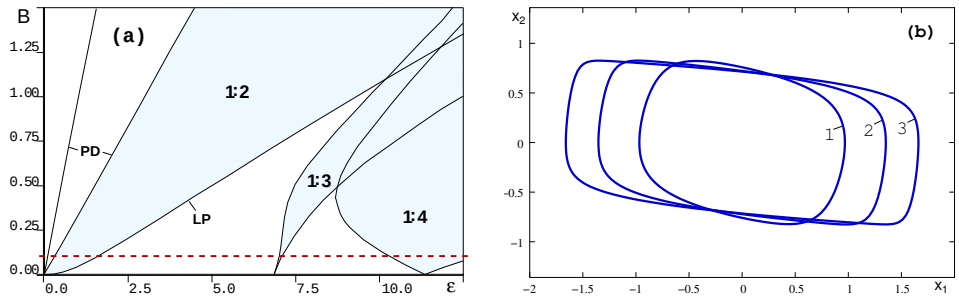

Figure 7: Simplified bifurcation diagram of the full system (18-20) in the (ε, B) parameter plane (a). The 1:2, 1:3 and 1:4 resonance tongues are drawn as shaded areas. We continued the invariant tori along the read dashed line at $B = 0.1$. Panel (b) shows limit cycles of subsystem (18-19) for $B = 0$ and $\varepsilon = 3.0$ (label 1), $\varepsilon = 6.5$ (label 2) and $\varepsilon = 9$ (label 3).

tori. To simplify the discussion, we write (17) as the first order system in extended phase space

$$\dot{x_1} = x_2, \tag{18}$$

$$\dot{x_2} = -(1 + B\sin\theta)\, x_1 + \left(\frac{\varepsilon}{2} - B\right) x_2 - (\varepsilon - B)x_2^3, \tag{19}$$

$$\dot{\theta} = 2, \tag{20}$$

where $\theta \in \mathbb{T}^1$. For $B = 0$ the sub-system (18-19) decouples from θ and it can be shown that a family γ_ε of limit cycles for (18-19) exists for $\varepsilon > 0$; see Fig. 7 (b). Thus, an ε-dependent family $T_{\varepsilon,0} := \gamma_\varepsilon \times \mathbb{T}^1$ of invariant tori with parallel flow exists for system (18-20), which are normally attracting for $\varepsilon > 0$. This implies that, for sufficiently small $B > 0$, a family $T_{\varepsilon,B}$ of normally hyperbolic invariant tori exists, which are either quasiperiodic or phase-locked.

Let $T_1 = \pi$ (so $\omega_1 = 2$) denote the forcing period, $T_2 = 2\pi/\omega_2$ the period of an element of γ_ε and $\varrho_\varepsilon := T_1/T_2 = \omega_2/\omega_1$ the rotation number. A resonance tongue in the (ε, B) parameter plane starts at each point $(\varepsilon, 0)$, where ϱ_ε is rational; see Fig. 7 (a). For simplicity, we only depicted the strong resonances, that is, resonances with $\varrho_\varepsilon \in \{1/1, 1/2, 1/3, 1/4\}$. Fig. 7 (a) shows a simplified bifurcation diagram of system (18-20) in the (ε, B)-parameter plane. The boundaries of the Arnol′d tongues are loci of limit-points. Within the white areas in between the 1:2, 1:3 and the 1:4 resonance tongues we can expect that quasiperiodic or weakly resonant tori exist.

5.2.2 Continuation of Tori

Using the proposed algorithm, we continued the invariant tori for fixed $B = 0.1$ (dashed red line in Fig. 7 (a)) with respect to ε in the interval $\varepsilon \in [1.7, 6.98]$ in between the 1:2 and 1:3 resonance tongues. During the continuation phase-locking will occur, but almost all of the resulting periodic orbits will have such high periods that, numerically, the flow can be regarded as quasiperiodic. As a seed solution we used the torus function $x_1(\theta_1, \theta_2) = \sin\theta_2$, $x_2(\theta_1, \theta_2) = \cos\theta_2$ together with the basic frequencies $\omega_1 = 2$ and $\omega_2 = 0.96$, which is an approximation to $\gamma_{2.0} \times \mathbb{T}^1$. We computed and continued numerical approximations of the tori on a fixed 41×101-mesh. The start value $\varepsilon = 2.0$ is chosen in order to be far enough away from the 1:2 resonance tongue and the choice $N_1 = 2.5N_2$ for the mesh consistently gave the best results.

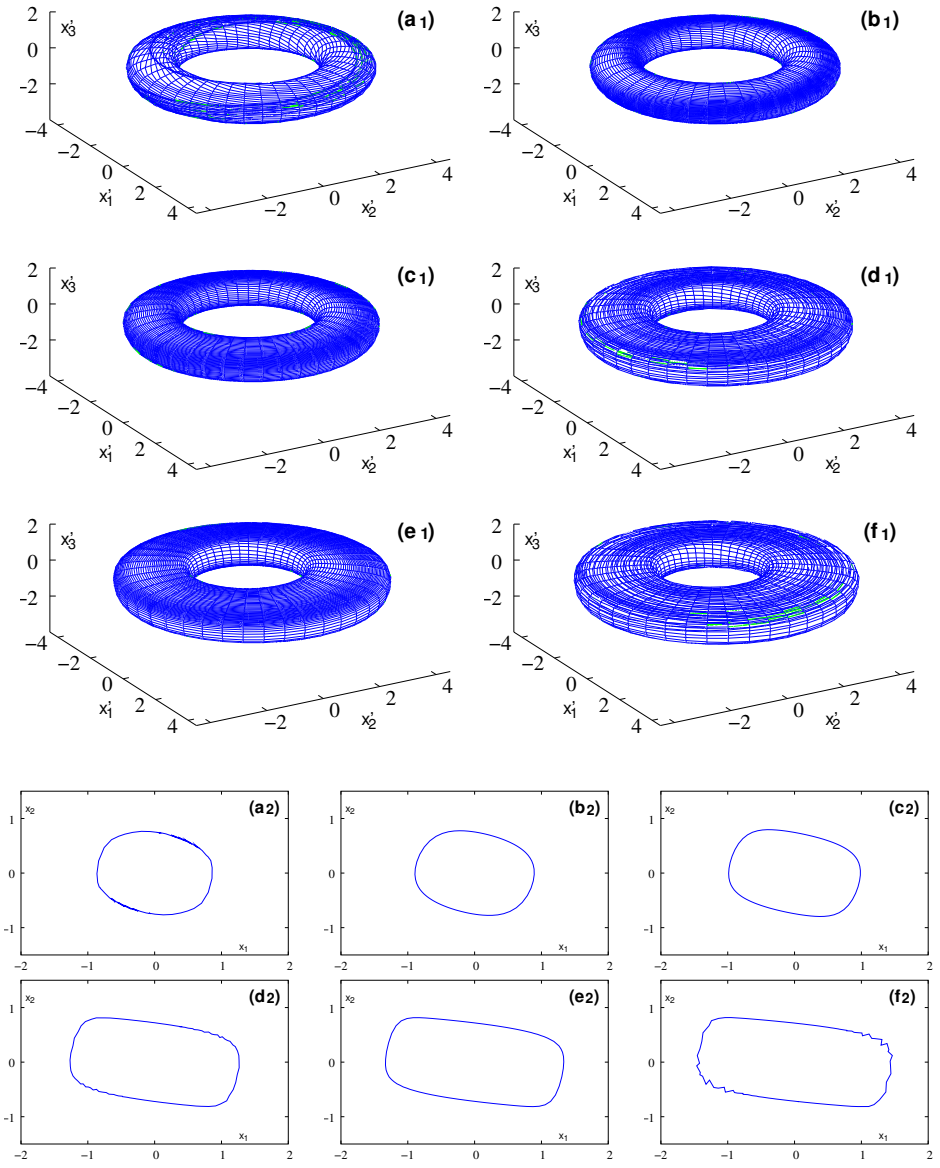

Figure 8: The invariant torus of system (18-20) together with cross sections at $\theta_1 = 0$ for $B = 0.1$ and $\varepsilon = 1.750$ (a_1, a_2), $\varepsilon = 2.000$ (b_1, b_2), $\varepsilon = 3.054$ (c_1, c_2), $\varepsilon = 5.493$ (d_1, d_2), $\varepsilon = 6.000$ (e_1, e_2) and $\varepsilon = 6.884$ (f_1, f_2), respectively. The tori are embedded into $\mathbb{R}^3$ by $x_1' = 3 + x_1 \cos\theta_1$, $x_2' = 3 + x_1 \sin\theta_1$ and $x_3' = x_2$. Even though it is very hard to see, in cross section (a_2) the mesh is actually overlapping itself.

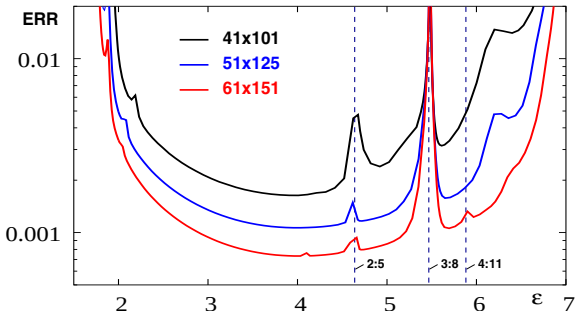

Figure 9: The estimated error measured via the parameter for different meshes, illustrating the typical convergence behaviour during a one-parameter continuation. The vertical lines indicate parameter values for which 'stronger' resonances occur. Note that these resonances belong to the Farey sequence $2/5 = 1/2 \oplus 1/3$, $3/8 = 2/5 \oplus 1/3$ and $4/11 = 3/8 \oplus 1/3$ [30].

Fig. 8 shows the invariant tori together with their cross-sections at $\theta_1 = 0$ for different parameter values ε; compare also the periodic orbits for $B = 0$ in Fig. 7 (b). Starting with an approximation at $\varepsilon = 2.0$, shown in panel (b_1), we first continued the torus for $1.7 \leq \varepsilon < 2.0$. As ε approaches the border of the 1:2 resonance tongue, the solution develops more and more ripples (see Fig. 8 (a_1)), and the estimated error grows rapidly as depicted in Fig. 9 (a). Subsequently, we continued the torus for $2.0 < \varepsilon \leq 6.98$. In the interval $\varepsilon \in [2, 5.4]$ the algorithm converges quickly and the solutions seem smooth, (c_1). For $\varepsilon \approx 5.5$ a 3:8 resonance occurs which visibly influences the algorithm. The estimated error in Fig. 9 (a) shows a very clear peak and the approximation is no longer smooth; see Fig. 8 (d_1). Furthermore, it takes a large number of continuation steps to pass through the resonance tongue. For $\varepsilon > 5.6$ the algorithm has no problems until the parameter approaches values near the border of the 1:3 resonance tongue at $\varepsilon \approx 7$. We observe the same behaviour as for the 1:2 resonance. Namely, the estimated error grows rapidly and the approximations are again non-smooth; see Fig. 8 (f_1).

Fig. 9 illustrates the typical convergence behaviour of our algorithm during a one-parameter continuation; compare with Fig. 3 (b). The estimated error is shown as a function of ε for mesh sizes 41×101, 51×125 and 61×151; see §4.1 for how the error is measured. The vertical dashed lines indicate selected values of ε for which resonances occur that affect the computation. Whenever the torus becomes resonant, we expect convergence problems because the torus is then phase-locked and our invariance equation does not hold. However, this does not necessarily mean that the algorithm breaks down; see §4.3. Namely, with the exception of the 3:8 resonance, 'weaker resonances' apparently do not influence the algorithm. There is a clear peak in the estimated error around $\varepsilon \approx 5.5$, which is exactly the point where ε crosses the 3:8 resonance line, but the algorithm still produces an acceptable approximation; see Fig. 8 panels (d_1, d_2). In comparison, the peaks near the 2:5 ($\varepsilon \approx 4.6$) and the 4:11 ($\varepsilon \approx 5.9$) resonances are far less pronounced. Other weak resonances have no observable effects at this numerical accuracy.

5.3 A circuit with saturable inductors

As our last example we numerically investigate a nonlinear electrical circuit given by Hayashi in [34]. The circuit is depicted in Fig. 10 and contains an oscillator built by the two saturable inductors I_1 and I_2, a capacitor C, a resistor R_1 and an AC voltage source S_1. Furthermore, a DC bias is superposed by the loop S_2-

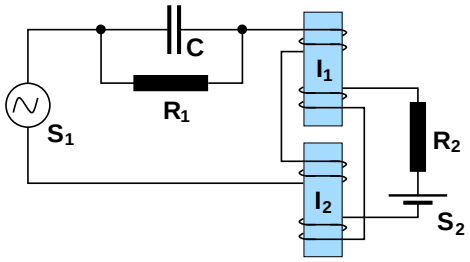

Figure 10: The resonant circuit with two saturable inductors (I_1 and I_2) described by system (21). In addition, the circuit contains an AC (S_1) and a DC (S_2) voltage source.

R_2-I_1-I_2 where S_2 is a DC voltage source and R_2 a further resistor. The nonlinear characteristics of the cores of I_1 and I_2 are assumed to be cubic and hysteresis is neglected. The ODEs modelling the circuit are

$$\left\{\begin{array}{rcl} \dot{x}_1 &=& x_2\,, \\ \dot{x}_2 &=& -k_1 x_2 - \frac{1}{8}(x_1^2 + 3x_3^2)x_1 + B\cos t\,, \\ \dot{x}_3 &=& -\frac{1}{8}k_2(3x_1^2 + x_3^2)x_3 + B_0\,, \\ \dot{t} &=& 1\,. \end{array}\right. \tag{21}$$

Here, $x \in \mathbb{R}^3$ and $B_0, B, k_1, k_2 \in \mathbb{R}$ are free parameters; see [34] and [69] for more details of the derivation. The values of the x_i are dimensionless quantities and do not correspond directly to particular currents or voltages of the circuit. For $x_3 \equiv 0$ and $B_0 = 0$ one obtains Duffing's equation, therefore, system (21) is sometimes referred to as being of Duffing type. System (21) was studied extensively in, for example, [34] and [69] using simulation and averaging and it was found that quasiperiodic invariant tori and, in particular, a sequence of torus-doubling bifurcations occur.

Let us be more precise by defining the term *torus-doubling bifurcation* in the spirit of Arnéodo, Coullet and Spiegel [1]. Suppose the ODE

$$\dot{x} = f(x,\mu)\,, \qquad f : \mathbb{R}^n \times \mathbb{R} \to \mathbb{R}\,, \tag{22}$$

with parameter μ has a periodic orbit that undergoes a period-doubling bifurcation for some $\mu_0 \in \mathbb{R}$. To every periodic orbit of (22) we can associate an invariant torus by adjoining the equation

$$\dot{\theta} = \omega\,, \qquad \theta \in \mathbb{T}^1\,. \tag{23}$$

The extended system (22-23) will exhibit a torus-doubling bifurcation at μ_0. Now consider the perturbed system

$$\left\{\begin{array}{rcl} \dot{x} &=& f(x,\mu) \;+\; \varepsilon g(x,\theta)\,, \\ \dot{\theta} &=& \omega \;+\; \varepsilon h(x,\theta)\,, \end{array}\right. \tag{24}$$

where ε is a positive parameter. For small ε the tori of (22-23) will persist, provided that these are sufficiently normally hyperbolic. However, at μ_0 these tori lose normal hyperbolicity. Hence, for small $\varepsilon \neq 0$ there exists a whole interval $[\mu_1, \mu_2]$ such that no normally hyperbolic torus exists in (24) for $\mu \in [\mu_1, \mu_2]$. For $\mu \notin [\mu_1, \mu_2]$ we still have the situation that on one side of the interval there exist only single tori whereas on the other side of the interval we have single and double tori. If the length of the interval is small, we refer to this phenomenon as a torus-doubling bifurcation.

It can be shown, that for sufficiently smooth right-hand sides of (24) the length of the interval $[\mu_1, \mu_2]$ decreases rapidly with ε, provided that the system can be separated into 'slow' and 'fast' variables; see [52]. This means for quasiperiodic tori that the basic frequencies must have sufficiently distinct values. This condition is met in our example and a crude but simple way to separate 'slow' and 'fast' variables is by averaging the system as described below. The sequence of torus doublings mentioned above is observed in simulations of (21) for the fixed parameter values $B_0 = 0.03$, $B = 0.22$, $k_2 = 0.05$ and varying $k_1 \in [0.04, 0.2]$. The aim of our investigation is to compute the invariant tori occurring in this system directly as a two-dimensional manifold.

By averaging, it is possible to derive a system that approximates (21) and where the variables x and t are decoupled. Suppose the solutions of (21) are almost harmonic oscillations with the same frequency as the voltage imposed by the voltage source S_1. Then we may assume that $x(t)$ takes the form

$$\left\{\begin{array}{rcl} x_1(t) &=& y_1(t)\cos t + y_2(t)\sin t\,, \\ x_2(t) &=& -y_1(t)\sin t + y_2(t)\cos t\,, \\ x_3(t) &=& y_3(t)\,, \end{array}\right. \tag{25}$$

with time-dependent amplitudes $y \in \mathbb{R}^3$. Using (25) one can derive the autonomous system

$$\left\{\begin{array}{rcl} \dot{y}_1 &=& \dfrac{1}{2}(-k_1 y_1 - A y_2)\,, \\ \dot{y}_2 &=& \dfrac{1}{2}(A y_1 - k_1 y_2 + B)\,, \\ \dot{y}_3 &=& B_0 - \dfrac{1}{16}k_2(3r^2 + 2y_3^2)y_3\,, \\ \dot{t} &=& 1\,, \end{array}\right. \tag{26}$$

where the 'slow' variables y and the 'fast' variable t are now decoupled; see also [69]. The additional quantities A and r are defined by

$$\begin{array}{rcl} A &:=& 1 - \dfrac{3}{32}(r^2 + 4y_3^2)\,, \\ r^2 &:=& y_1^2 + y_2^2\,. \end{array}$$

5.3.1 Numerical Analysis

The bifurcation diagram of the averaged system (26) can be computed with AUTO [23]; see Fig. 11 (a). The black curve marked by label 1 is a family of equilibrium points. For decreasing $k_1 < 0.2$ the equilibria lose stability at $k_1 \approx 0.1189$ in a Hopf bifurcation (label 2) and a family of attracting periodic orbits branches off (blue). In panel (b) an orbit of this family is shown for $k_1 = 0.09$. At $k_1 \approx 0.0772$ the periodic orbits lose stability in a period-doubling bifurcation (label 4) and a family of doubled periodic orbits emanates. At $k_1 \in \{0.0509,\, 0.0476,\, \dots\}$ further period doublings occur that apparently form a cascade. Orbits of the doubled and quadrupled families are shown in panels (c) and (d) for $k_1 = 0.06$ and $k_1 = 0.05$, respectively.

According to transformation (25) an equilibrium point of the averaged system (26) corresponds to a periodic orbit of the full system (21). Therefore, we expect a family of periodic orbits in the full system (21) close to the branch of equilibria of system (26). From the occurrence of a Hopf bifurcation at label 2 in the averaged system we conclude that in the full system the family of periodic orbits undergoes a torus bifurcation near $k_1 \approx 0.1189$ and that a family of invariant tori emanates. Similarly, we expect that the period-doubling bifurcations of the averaged system

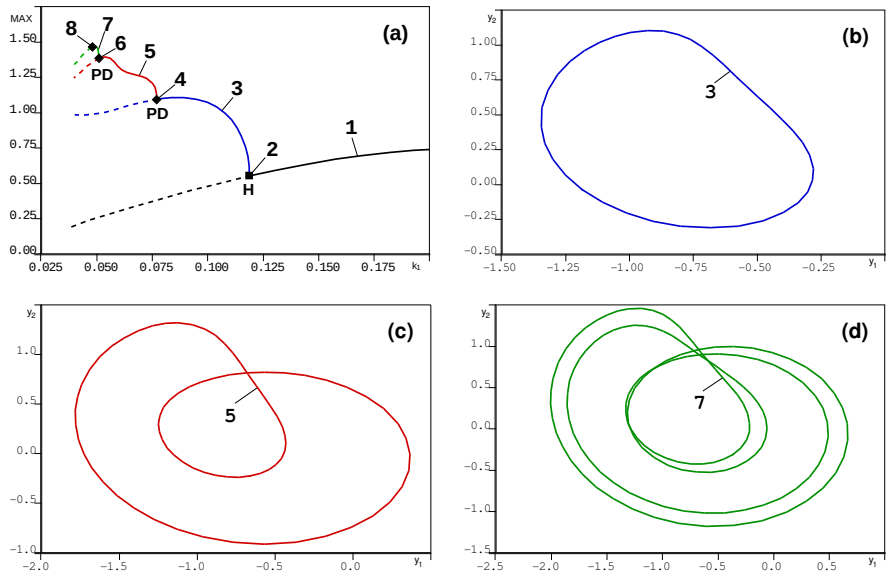

Figure 11: The bifurcation diagram of system (26) with the maximum of y_2 versus k_1 (a). The black line marked by label 1 is a branch of equilibrium points. For decreasing k_1 a family of periodic orbits (blue) branches off in a Hopf bifurcation at label 2. It seems that for decreasing k_1 a cascade of period-doubling bifurcations occur, the start of which is indicated in panel (a) by the labels 4, 6 and 8. The attracting periodic orbits for $k_1 = 0.09$ (label 3), $k_1 = 0.06$ (label 5) and $k_1 = 0.05$ (label 7) are shown in panels (b), (c) and (d), respectively, projected into the (y_1, y_2)-plane. For $k_1 \approx 0.04$ a strange attractor is observed in simulations.

at labels 4, 6, 8, etc. in Fig. 11 correspond to torus-doubling bifurcations at 'nearby values' of k_1 in the full system. In fact, in simulations we observe quasi-periodic orbits and a rather long sequence of torus doublings which seems to result in a strange attractor. Moreover, the invariant circles of the period-2π stroboscopic map have a shape similar to the periodic orbits shown in Fig. 11 (b)-(c); see also [69].

In general, one observes finite and typically short sequences of torus doublings. Since the intervals $[\mu_1, \mu_2]$ where the tori lose normal hyperbolicity have finite non-zero length, close to the 'accumulation point' these 'bifurcation intervals' are not disconnected. Thus, our definition of the term 'torus doubling' does not apply. Some numerical results regarding sequences of torus doublings can be found in [65], in particular, the term 'doubling of a destroyed torus' is defined. In the example discussed here, it is not yet clear whether one observes doublings of tori or of thin 'destroyed tori' that look like torus doublings and, therefore, create the impression of a long torus-doubling sequence.

5.3.2 Continuation of Tori

It is possible to compute the family of periodic orbits (black curve in Fig. 12 (a)) of the full system (26) with AUTO [23] whereby a torus bifurcation is detected at $k_1 \approx 0.1214$ (label 2). Using our algorithm we can complete this bifurcation diagram by branches of tori (blue and red), including the parts of the branches where the tori are of saddle-type (dashed). Note, that these tori cannot be obtained by simulation. The bifurcation diagram is shown in Fig. 12 (a) and the branches are labelled in the same way as in Fig. 11 (a). These two bifurcation diagrams appear to be very similar which is numerical evidence that the qualitative analysis using the averaged

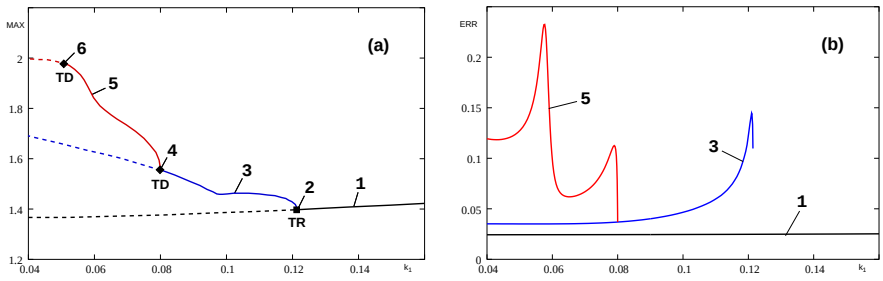

Figure 12: The bifurcation diagram of system (21) with $\max_{\theta\in\mathbb{T}^2}\{|u_1(\theta)|, |u_2(\theta)|\}$ versus k_1 (a). The black curve marked by label 1 is a branch of periodic orbits. For decreasing k_1 a family of invariant tori (blue, label 3) branches off in a torus bifurcation at $k_1 \approx 0.1214$ (label 2). The invariant tori of this family undergo a torus-doubling bifurcation at $k_1 \approx 0.0799$ (label 4) and a family of doubled invariant tori emanates (red, label 5). As k_1 decreases further, more torus-doubling bifurcations are found, for example at $k_1 \approx 0.0517$ (label 6), which seem to form a cascade similar to the cascade of period doublings found in system (26). Panel (b) shows the estimated error for each branch of the bifurcation diagram (a), which was monitored as a function of k_1.

system (26) is accurate for this system and the choice of parameter values.

Fig. 13 shows the primary and Fig. 14 the doubled tori for different parameter values. The torus in Fig. 13 (a) is close to the torus bifurcation and, therefore, almost coincides with the unstable periodic orbit inside it. In Fig. 14 we left out part of the tori and highlighted a cross-section. This cross-section is actually an approximation to the invariant closed curve of the period-2π stroboscopic map of the full system (21); see §3. Hence, it is similar to the doubled periodic orbits of the averaged system (26); see also Fig. 11 (c). The self-intersection of the doubled tori is due to the projection of the tori from the 4-dimensional phase space $\mathbb{R}^3 \times \mathbb{T}^1$ into the 3-dimensional (x_1, x_2, x_3)-space, which is also a Poincaré section of the phase space for fixed $\theta \in \mathbb{T}^1$.

The branches of invariant tori were computed as follows. We obtained seed approximations of the primary and doubled invariant tori by two dimensional Fourier analysis of simulation data obtained for $k_1 = 0.09$ (primary torus) and $k_1 = 0.0775$ (doubled torus), respectively, and continued the branches in both directions. The tori were computed on a 31×31 mesh (primary torus) and a 31×61 mesh (double torus), respectively. Unlike the previous example, we do not encounter convergence problems caused by strong resonances because the rotation numbers vary between $\rho_{k_1} \in [0.093, 0.132]$ for the primary tori and $\rho_{k_1} \in [0.053, 0.074]$ for the doubled tori. The parameter values at which the torus-doubling bifurcations occur were obtained by investigation of the simulation as well as the continuation data.

The convergence behaviour of our algorithm depending on the parameter is illustrated in Fig. 12 (b). It shows the graphs of the estimated error along each branch as functions of the parameter k_1. The error remains bounded and the occurring peaks are not high compared to the average error of each branch. The error is relatively large, but this is due to the coarse meshes used; the solutions themselves seem smooth for all parameter values.

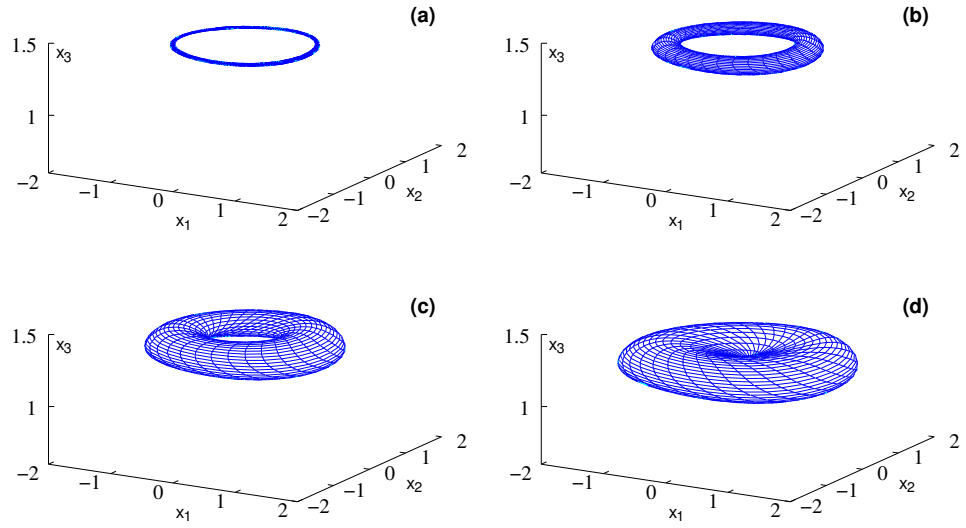

Figure 13: The primary invariant torus of system (21) for $k_1 = 0.1214$ (a), $k_1 = 0.1182$ (b), $k_1 = 0.1044$ (c), and $k_1 = 0.0444$ (d), respectively, projected onto (x_1, x_2, x_3)-space. For decreasing k_1 the torus separates rapidly from the periodic orbit and becomes 'fatter'. Note that the torus in panel (d) is of saddle type.

6 Conclusion

In this paper, we proposed a natural parametrisation of quasiperiodic invariant tori, which was obtained by imposing that the flow on the torus be in normal form, that is, diffeomorphic to a parallel flow. The discretisation of the corresponding invariance equation by finite-differences led to algorithms of high order of consistency that can be constructed by recursion over the dimension p of the torus. Full proofs of well-posedness and convergence are still open. The algorithm is implemented as a corrector in both, a p- and a one-parameter continuation environment. The continuation of quasiperiodic invariant tori with respect to p parameters is well defined and the correct setting for detecting local quasiperiodic bifurcations. On the other hand, continuation with respect to one parameter is problematic, because here, the tori are generally phase-locked. Nevertheless, as was illustrated with examples, a one-parameter continuation is possible, provided that the encountered resonances are 'weak enough'. The algorithm is independent of the stability type of the computed torus and able to 'step over' regions where the torus changes stability, as was demonstrated in the last example.

7 Acknowledgements

The authors are grateful to the anonymous referees; their suggestions substantially improved this paper. We would like to thank Bernd Krauskopf and Alan Champneys for their careful reading of and constructive suggestions on a draft of this paper. Considerable credit goes to them and also to Jan Sieber for inspiring discussions and valuable hints. We are particularly grateful to Àngel Jorba and Henk Broer for their help on algorithms for Hamiltonian systems and references to constructive KAM theorems. This work was supported by EPSRC grant GR/R72020/01.

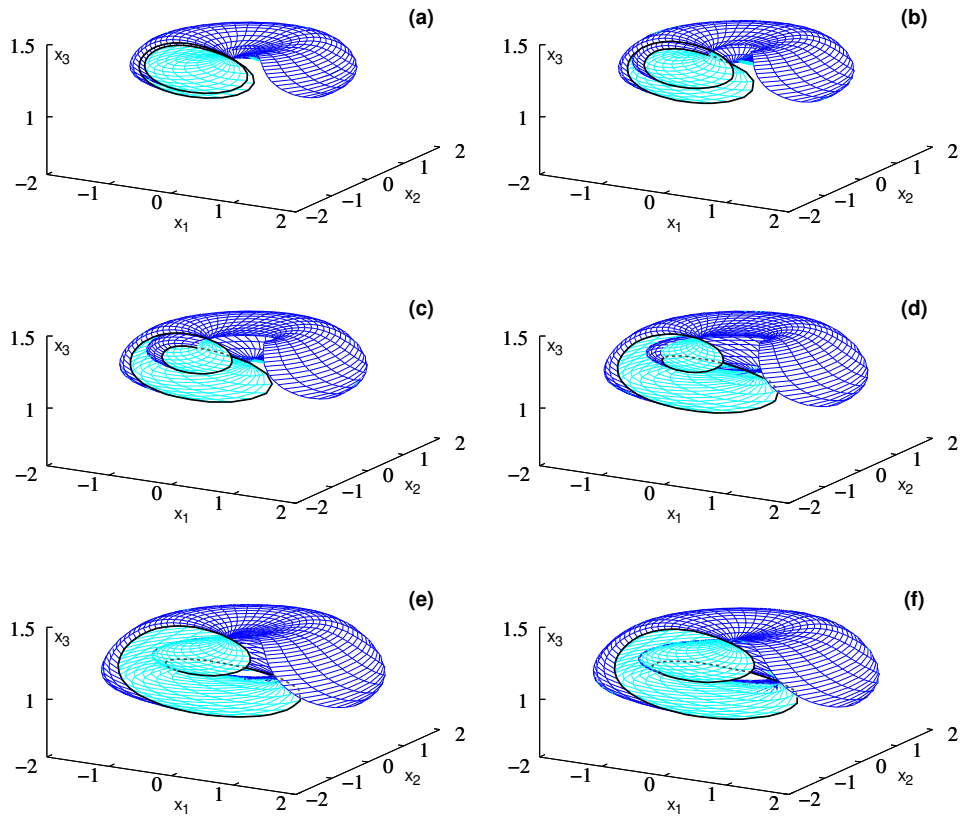

Figure 14: The doubled invariant torus of system (21) for $k_1 = 0.0797$ (a), $k_1 = 0.0775$ (b), $k_1 = 0.0700$ (c), $k_1 = 0.0598$ (d), $k_1 = 0.0502$ (e), and $k_1 = 0.0421$ (f), respectively, projected onto (x_1, x_2, x_3)-space. Only part of the tori is shown and a cross-section is drawn as a black curve to emphasise the evolution of the tori. The behaviour of the cross-section is qualitatively similar to the behaviour observed in period-doubling bifurcations of periodic orbits. Note that the tori shown in panels (e) and (f) are of saddle type. The self intersection of the tori is due to projection.

8 Contact

Frank Schilder, Bristol Centre for Applied Nonlinear Mathematics, Department of Engineering Mathematics, University of Bristol, Bristol BS8 1TR, UK
(f.schilder@bristol.ac.uk)

Hinke M. Osinga, Bristol Centre for Applied Nonlinear Mathematics, Department of Engineering Mathematics, University of Bristol, Bristol BS8 1TR, UK
(h.m.osinga@bristol.ac.uk)

Werner Vogt, Technische Universität Ilmenau, Fakultät für Mathematik und Naturwissenschaften, Postfach 100565, 98684 Ilmenau, Germany
(werner.vogt@mathematik.tu-ilmenau.de)

References

[1] A. Arnéodo, P.H. Coullet and E.A. Spiegel, *Cascade of period doublings of tori*, Phys. Lett. A 94, 1 (1983), pp. 1–6.

[2] V.I. Arnol′d, *Small denominators. I. Mappings of the circumference to itself*, Izv. Akad. Nauk SSSR, Ser. Mat., 26 (1961), pp. 21–86; English translation, Amer. Math. Soc. Transl., 46 (1965), pp. 213–284.

[3] S. Bauer, O. Brox, J. Kreissl, B. Sartorius, M. Radziunas, J. Sieber, H.J. Wünsche and F. Henneberger, *Nonlinear dynamics of semiconductor lasers with active optical feedback*, Physical Review E, 69 (2004), 016206.

[4] K. Bernet and W. Vogt, *Anwendung finiter Differenzenverfahren zur direkten Bestimmung invarianter Tori*, ZAMM, 74(6) (1994), pp. T577–T579.

[5] P. Bonello, M.J. Brennan and R. Holmes, *Non-linear modelling of rotor dynamic systems with squeeze film dampers — an efficient integrated approach*, J. Sound and Vib., 249(4) 2002, pp. 743–773.

[6] H.W. Broer, *Quasi-periodic bifurcations, applications*, Proceedings of the XIth Congress on Differential Equations and Applications/First Congress on Applied Mathematics (Spanish) (Ma'laga, 1989), pp. 3–21, Univ. Ma'laga, Ma'laga, 1990.

[7] H.W. Broer, A. Hagen, and G. Vegter, *Multiple purpose algorithms for invariant manifolds*, Second International Conference on Dynamics of Continuous, Discrete and Impulsive Systems (London, ON, 2001). Dyn. Contin. Discrete Impuls. Syst. Ser. B Appl. Algorithms 10(1-3), 2003, pp. 331–344.

[8] H.W. Broer, G.B. Huitema and M.B. Sevryuk, *Quasi-Periodic Motions in Families of Dynamical Systems*, Springer-Verlag Berlin, 1996.

[9] H.W. Broer, G.B. Huitema, F. Takens and B.L.J. Braaksma, *Unfoldings and bifurcations of quasi-periodic tori*, Mem. Amer. Math. Soc. 83(421) (1990), viii+175 pp.

[10] H.W. Broer, H.M. Osinga and G. Vegter, *Computing a normally hyperbolic invariant manifold of saddle type*, in G.S. Ladde and M. Sambandham, eds., Proceedings of Dynamic Systems & Applications 2, Dynamic Publishers, 1996, pp. 83–90.

[11] ———, *On the computation of normally hyperbolic invariant manifolds*, in H.W. Broer, S.A. van Gils, I. Hoveijn and F. Takens, eds., Nonlinear Dynamical Systems and Chaos, Progress in Nonlinear Differential Equations and Their Applications 19, Birkhäuser Verlag, Basel / Switzerland, 1996, pp. 423–447.

[12] ———, *Algorithms for computing normally hyperbolic invariant manifolds*, ZAMP, 48(3) (1997), pp. 480–524.

[13] ———, *Computing a normally attracting invariant manifold of a Poincaré map*, in P.L. Butzer, H.Th. Jongen, and W. Oberschelp, eds., Charlemagne and His Heritage, 1200 Years of Civilization and Science in Europe, Volume 2: Mathematical Arts, Brepols Publishers, 1998, pp. 541–549.

[14] W.G. Büntig and W. Vogt, *Numerical Bifurcation Analysis of Nonlinear Power Systems*, Proceedings of the 48th Internationales Wiss. Kolloquium, Technische Universität Ilmenau, 22.-25.9.2003, pp. 373–374.

[15] E. Castellà and À. Jorba, *On the vertical families of two-dimensional tori near the triangular points of the Bicircular problem*, Celestial Mech. 76(1) (2000), pp. 35–54.

[16] A. Celletti and C. Luigi, *A constructive theory of Lagrangian tori and computer-assisted applications*, Dynamics reported, Dynam. Report. Expositions Dynam. Systems (N.S.), 4, Springer, Berlin, 1995, pp. 60–129.

[17] L.O. Chua and A. Ushida, *Algorithms for computing almost periodic steady-state response of nonlinear systems to multiple input frequencies*, IEEE Trans. Circuits and Systems, 28(10) (1981), pp. 953–971.

[18] L. Debraux, *Numerical computation of a branch of invariant circles starting at a Hopf bifurcation point*, Contemp. Math., 172 (1994), pp. 169–184.

[19] L. Dieci, J. Lorenz and R.D. Russell, *Numerical calculation of invariant tori*, SIAM J. Sci. Stat. Comput., 12 (1991), pp. 607–647.

[20] L. Dieci and J. Lorenz, *Block M-matrices and computation of invariant tori*, SIAM J. Sci. Stat. Comput., 13 (1992), pp. 885–903.

[21] ———, *Computation of invariant tori by the method of characteristics*, SIAM J. Num. Anal., 32(5) (1995), pp. 1436–1474.

[22] C. Díez, À. Jorba and C. Simó, *A dynamical equivalent to the equilateral libration points of the real Earth-Moon system*, Celestial Mech. 50(1) (1991), pp. 13–29.

[23] E.J. Doedel, A.R. Champneys, Th.F. Fairgrieve, Y.A. Kuznetsov, B. Sandstede and X. Wang, *AUTO 97*: *Continuation and Bifurcation Software for Ordinary Differential Equations* (*with HomCont*), 1997

[24] E.J. Doedel, W. Govaerts, Y.A. Kuznetsov, *Computation of periodic solution bifurcations in ODEs using bordered systems*, SIAM J. Numer. Anal., 41(2) (2003), pp. 401–435.

[25] K.D. Edoh, R.D. Russell and W. Sun, *Computation of invariant tori by orthogonal collocation*, Applied Numerical Mathematics, 32 (2000), pp. 273–289.

[26] L.C. Evans, *Partial Differential Equations*, American Mathematical Society, Providence, Rhode Island, 1998.

[27] N. Fenichel *Persistence and smoothness of invariant manifolds for flows*, Indiana Univ. Math. J., 21 (1971), pp 193–226.

[28] F. Gabern and À. Jorba, *Effective computation of the dynamics around a two-dimensional torus of a Hamiltonian system*, Dynamical systems group preprint 3 (http://www.maia.ub.es/dsg/2004/), University of Barcelona, 2004.

[29] T. Ge and A.Y.T. Leung, *Construction of invariant torus using Toeplitz Jacobian matrices/fast Fourier transform approach*, Nonlinear Dynamics, 15 (1998), pp. 283–305.

[30] J.A. Glazier and A. Libchaber, *Quasi-periodicity and dynamical systems*: *An experimentalists view*, IEEE Trans. Circ. Sys., 35(7) (1988), pp. 790–809.

[31] G. Gómez, À. Jorba, J. Masdemont and C. Simó, *Dynamics and mission design near libration points, Vol. IV, Advanced methods for triangular points*, World Scientific Monograph Series in Mathematics 5, World Scientific Publishing Co. Inc., 2001.

[32] J. Guckenheimer and P. Holmes, *Nonlinear Oscillations, Dynamical Systems and Bifurcation of Vector Fields*, Springer-Verlag Berlin, 1997.

[33] W. Hackbusch, *Elliptic Differential Equations*, *Theory and Numerical Treatment*, Teubner Verlag Stuttgart, 1987; English translation, Springer Verlag Berlin Heidelberg, 1992.

[34] C. Hayashi, *Quasi-periodic oscillations in non-linear control systems*, in Selected Papers on Nonlinear Oscillations, Chihiro Hayashi, Professor Emeritus, Kyoto University; Kyoto University 1975, Printed by Nippon Printing and Publishing Company, Ltd. Yoshino, Fukushima-ku, Osaka, Japan.

[35] M. Hermann, *Numerische Mathematik*, R. Oldenbourg Verlag, Munich, 2001.

[36] M.W. Hirsch, C.C. Pugh, M. Shub, *Invariant manifolds*, Lecture Notes in Mathematics, Vol. 583. Springer-Verlag Berlin-New York, 1977.

[37] W. Ji and V. Venkatasubramanian, *Dynamics of a minimal power system*: *invariant tori and quasi-periodic motions*, IEEE Trans. Circuits Systems I Fund. Theory Appl., 42(12) (1995), pp. 981–1000.

[38] À. Jorba, *A methodology for the numerical computation of normal forms, centre manifolds and first integrals of Hamiltonian systems*, Experiment. Math., 8(2) (1999), pp. 155–195.

[39] À. Jorba, *Numerical computation of the normal behaviour of invariant curves of n-dimensional maps*, Nonlinearity 14(5) (2001), pp. 943–976.

[40] À. Jorba and J. Masdemont, *Dynamics in the centre manifold of the collinear points of the Restricted Three Body Problem*, Phys. D 132 (1999), pp. 189–213.

[41] Chr. Kaas-Petersen, *Computation of quasiperiodic solutions of forced dissipative systems*, J. Comput. Phys., 58(3) (1985), pp. 395–408.

[42] ———, *Computation of quasiperiodic solutions of forced dissipative systems. II*, J. Comput. Phys., 64(2) (1986), pp. 433–442.

[43] ———, *Computation, continuation, and bifurcation of torus solutions for dissipative maps and ordinary differential equations*, Phys. D, 25(1-3) (1987), pp. 288–306.

[44] I.G. Kevrekidis, R. Aris, L.D. Schmidt and S. Pelikan, *Numerical computations of invariant circles of maps*, Physica D, 16 (1985), pp. 243–251.

[45] B. Krauskopf, N. Tollenaar and D. Lenstra, *Tori and their bifurcations in an optically injected semiconductor laser*, Optics Communications, 156(1-3) (1998), pp. 158–169.

[46] B. Krauskopf, S.M. Wieczorek and D. Lenstra, *Different types of chaos in an optically injected semiconductor laser*, Applied Physics Letters, 77(11) (2000), pp. 1611–1613.

[47] R. de la Llave and D. David, *Accurate strategies for small divisor problems*, Bull. Amer. Math. Soc. (N.S.), 22(1) (1990), pp. 85–90.

[48] R. de la Llave, *A tutorial on KAM theory*, in Smooth ergodic theory and its applications (Seattle, WA, 1999), Proc. Sympos. Pure Math., 69, Amer. Math. Soc., Providence, RI, 2001, pp. 175–292.

[49] P. Lenas, N.A. Thomopoulos, D.V. Vayenas and S. Pavlou, *Oscillations of two competing microbial populations in configurations of two interconnected chemostats*, Math. Biosci., 148(1) (1998), pp. 43–63.

[50] H. Mingyou, T. Küpper and N. Masbaum, *Computation of invariant tori by the Fourier methods*, SIAM J. Sci. Comput., 18 (1997), pp. 918–942.

[51] G. Moore, *Computation and parametrisation of invariant curves and tori*, SIAM J. of Numer. Anal., 33(6) (1996), pp. 2333–2358.

[52] A.I. Neishtadt, *The separation of motions in systems with rapidly rotating phase*, J. Appl. Math. Mech., 48(2) (1985), pp. 133–139; translated from Prikl. Mat. Mekh., 48(2) (1984), pp. 197–204 (Russian).

[53] N. Nicolaisen, B. Werner, *Discretisation of circle maps*, Z. Angew. Math. Phys., 49(6) (1998). pp. 869–895.

[54] H.M. Osinga: Computing Invariant Manifolds: Variations on the Graph Transform, Diss., Univ. Groningen, 1996.

[55] S. Östlund, D. Rand, J. Sethna and E. Siggia, *Universal properties of the transition from quasiperiodicity to chaos in dissipative systems*, Phys. D, 8(3) (1983), pp. 303–342.

[56] T.S. Parker and L.O. Chua, *Practical Numerical Algorithms for Chaotic Systems*, Springer-Verlag New York, 1989.

[57] E. Philippow and W.G. Büntig, *Analyse nichtlinearer dynamischer Systeme der Elektrotechnik*: *Einführung in die numerische Untersuchung einfacher Systeme*, Carl Hanser Verlag München et al., 1992.

[58] V. Reichelt, *Computing invariant tori and circles in dynamical systems*, in E.J. Doedel and L.S. Tuckermann, eds., Numerical Methods for Bifurcation Problems and Large-Scale Dynamical Systems, IMA Volumes in Mathematics and its Applications 119 pp. 407–437, Springer Verlag, 2000.

[59] W.C. Rheinboldt, *Numerical analysis of parameterized nonlinear equations*, Wiley New York, 1986.

[60] Y. Saad, *SPARSKIT: A basic tool kit for sparse matrix computations*, technical report No. RIACS-90-20, Research Institute for Advanced Computer Science, NASA Ames Research Center, Moffett Field, CA, 1990.

[61] A.M. Samoilenko, *Elements of the Mathematical Theory of Multi-Frequency Oscillations*, Isdatelstvo Nauka, Moskva 1987; English translation, Kluwer Academic Publishers, Dordrecht et al., 1991.

[62] F. Schilder, *Numerische Approximation quasiperiodischer invarianter Tori unter Anwendung erweiterter Systeme*, Dissertation, TU Ilmenau, 2004; elektronische Veröffentlichung unter `http://www.db-thueringen.de/servlets/DocumentServlet?id=2058`.

[63] F. Schilder, *TorCont: computation and continuation of quasiperiodic invariant tori*, software package, `http://www.dynamicalsystems.org/sw/sw/detail?item=44`.

[64] C. Simó, *Effective computations in celestial mechanics and astrodynamics*, in Modern Methods of Analytical Mechanics and their Applications, CISM Courses and Lectures 387, V.V. Rumyantsev and A.V. Karapetyan, eds., Springer Verlag, 1998.

[65] J.J. Stagliano, J.-M. Wersinger, E. Slaminka, *Doubling bifurcations of destroyed $\mathbb{T}^2$ tori*, Phys. D 92(3-4) (1996), pp. 164–177.

[66] M. van Veldhuizen, *A new algorithm for the numerical approximation of an invariant curve*, SIAM J. Sci. Stat. Comput., 8 (1987), pp. 951–962.

[67] ———, *Convergence results for invariant curve algorithms*, Math. Comp., 51(184) (1988), pp. 677–697.

[68] S. Wiggins, *Normally Hyperbolic Invariant Manifolds in Dynamical Systems*, Springer-Verlag, 1994.

[69] T. Yoshinaga and H. Kawakami, *Bifurcations and chaotic state in forced oscillatory circuits containing saturable inductors*, In: T. Carroll and L. Pecora, Nonlinear Dynamics In Circuits, pp. 89–118, World Scientific Publishing, 1995.